Reaction Chemistry & Engineering

ROYAL SOCIETY OF CHEMISTRY

PAPER

View Article Online
View Journal | View Issue

Cite this: *React. Chem. Eng.*, 2026, 11, 234

Thermodynamic model for synergistic solvent extraction of mineral acids by tris(2-ethylhexyl) amine and 1-octanol

Rayco Lommelen * and Koen Binnemans

Received 2nd September 2025,
Accepted 10th October 2025

DOI: 10.1039/d5re00386e

rsc.li/reaction-engineering

Recovery of excess acid after leaching is essential in circular hydrometallurgical processes, because it reduces reagent consumption and generates less waste. Solvent extraction can be used for acid recovery from aqueous solutions. This study presents a thermodynamic model for the synergistic solvent extraction of H_2SO_4, HCl, and methanesulphonic acid (MSA) using tris(2-ethylhexyl)amine (TEHA) and 1-octanol in *n*-dodecane. The model is developed using the mixed-solvent electrolyte (MSE) framework of OLI Systems, integrating an extensive set of own experimental data and literature data. It captures both individual and synergistic extraction behaviours and accurately calculates equilibrium properties such as acid distribution, water uptake by the solvent, volume change during extraction, and organic phase mass density at room and elevated temperatures. Validation with H_2SO_4 recovery from $NiSO_4$ solutions confirms its predictive capabilities for industrially relevant conditions. This work offers a robust tool for designing acid recovery processes through solvent extraction and gives mechanistic insights into the studied extractant systems.

1. Introduction

Hydrometallurgical flowsheets often involve leaching with mineral acids, and an excess of acid is present after the leaching operation has finished.[1] Also, bleed streams of spent electrolyte from copper electrorefining or zinc electrowinning operations, as well as spent steel pickling solutions, contain large amounts of acids.[2,3] Neutralising these acids by adding a base results in a larger chemical consumption and produces salts or metal hydroxide precipitates that are typically classified as waste. This undermines the environmental benefits of the shift to climate neutrality, which requires hydrometallurgical flowsheets to purify the energy-transition metals. Sulphuric acid is most frequently used in hydrometallurgy, while chloride-based processes are also common.[4] Methanesulphonic acid (MSA) is less known in hydrometallurgy, but it has appealing properties for the development of circular hydrometallurgical flowsheets.[5,6]

Recovery of mineral acids can lower the environmental impact. This can be done either directly through, for example, a solvent extraction or membrane-based process for the recovery of the acid or through neutralisation of the acid and thermal decomposition of the salt in its acid and base (*e.g.* pyrohydrolysis).[2,7] Solvent extraction (SX) processes offer high productivity and low waste generation for acid recovery, but their design is complicated due to the need for several integrated stages (extraction, scrubbing, and stripping) and complex chemical processes.[8] The aqueous feed can contain high concentrations of acid and dissolved salts. The targeted acid then distributes to an immiscible organic phase that contains one or more extractants with a certain selectivity for that acid, through mixing both phases. This organic phase sometimes also contains a diluent to lower the viscosity and a phase modifier to stabilise the organic phase and avoid third-phase formation.

Trialkylamines (*e.g.*, trioctylamine (TOA) and tris(2-ethylhexyl)amine (TEHA)), organophosphates (*e.g.*, tri-*n*-butyl phosphate (TBP)), and phosphine oxides (*e.g.* trioctylphosphine oxide, and the commercial mixture Cyanex 923) have good properties for the extraction of mineral acids.[9–11] Literature on MSA extraction is sparse. A limited study on extraction by TOA,[12] a study on volume changes and water uptake in a MSA–tributyl phosphate system,[13] and a master's thesis on MSA recovery by TEHA and 1-octanol,[14] have been identified. The study demonstrates that the TEHA + 1-octanol system is highly effective for MSA recovery, offering strong extraction performance, efficient stripping, rapid phase separation, and no third-phase formation. Heidari *et al.* further show that this system is also suitable for H_2SO_4 recovery, outperforming TOA at higher acid concentrations and enabling easier stripping through dilution.[15] Stripping efficiencies would probably be too low if a modifier like 1-octanol were present. Addition of 1-octanol to trialkylamines has a dual function in these systems: it avoids third-phase formation and increases the extraction

KU Leuven, Department of Chemistry, Celestijnenlaan 200F, P.O. box 2404, B-3001 Leuven, Belgium. E-mail: rayco.lommelen@kuleuven.be

efficiency of acids.[14,16,17] At least for the extraction of MSA and H_2SO_4, mixtures of TEHA and 1-octanol exhibit synergy, *i.e.*, the extraction performance of the mixture exceeds the sum of the individual extractant contributions. TEHA, without 1-octanol or any modifier, can also be used as an extractant for HCl recovery.[18]

The availability of a robust and predictive thermodynamic model can support the design of complex solvent extraction processes. Such a model should be built on a thermodynamic framework that can capture the non-ideal interactions in mixed solvent–electrolyte systems. The thermodynamic modelling of solvent extraction processes has gone from purely empirical to frameworks that account for non-ideality in both aqueous and organic phases. Early empirical models fit purely mathematical equations to distribution data.[19–21] They do not take chemistry into account, which results in a lack of predictive power outside their calibrated conditions. Chemical reaction-based models introduce equilibrium constants to describe extraction reactions but still rely on concentrations rather than activities. This often results in the need to include hypothetical chemical species to account for non-ideal behaviour. Statistical thermodynamics offers, in principle, a rigorous route based on first principles, but the complexity of mixed-solvent–electrolyte systems renders this impractical for routine process design.[22–25] Practical implementations use semi-empirical activity models based on physical chemistry to convert concentrations to activities. Examples include the Pitzer equations for the aqueous phase and Margules, NRTL, or UNIQUAC approaches for the organic phase.[26,27] However, these often treat the organic phase as ideal or employ separate frameworks for each phase, failing to capture the non-ideal behaviour of the organic phase at significant extractant loading or the coupled non-ideal behaviour of the same electrolytes in both the aqueous and organic phases.[27–30]

A more unified, predictive framework can be found in mixed-solvent electrolyte (MSE) models, which describe both aqueous and organic phases within a single thermodynamic formalism. For instance, OLI systems' MSE model has been used to build thermodynamic models for acid and metal extraction from dilute solute and extractant conditions to higher concentrations and maximum loading capacities.[31–35] This framework considers speciation changes to represent chemical reactions, solid–liquid and vapour–liquid equilibria, and combines this with a three-term activity equation that also governs the liquid–liquid equilibria.[36,37] These three terms account for long-range electrostatic interactions through the Pitzer–Debye–Hückel formula, middle-range interactions through a second-virial-coefficient-type expression, and short-range interactions through the UNIQUAC equations. The interaction parameters in the middle- and short-range are determined through fitting to experimental data.

The framework uses a standard state defined at infinite dilution. The chemical potential of a species (μ_i) at conditions deviating from this standard state is corrected by the activity equations. The distribution of a species in a heterogeneous system at liquid–liquid equilibrium is constrained by the necessity for equal μ_i in each phase. The solution density can also be calculated based on single-species molar volumes and an equation for excess volume corrections. This is valuable for converting the mole- and mole-fraction-based units from the thermodynamic framework in g L^{-1} and mol L^{-1}, which are often encountered in hydrometallurgy.

Complementary approaches for activity corrections in mixed-solvent electrolyte systems, such as the mean-spherical approximation – NRTL model, combine the mean-spherical approximation for ionic interactions with a modified NRTL term.[38] This seems to work well, but is only applied to ternary systems with a fully dissociated salt, water, and solvent. Chemical reactions and density correlations, important to describe solvent extraction systems, are not incorporated. Also, perturbed chain statistical associating fluid theory (PC-SAFT) based equations of state show promising results to calculate mixed-solvent electrolyte systems.[39,40] They have possibly an improved physicochemical basis, but to the best of the authors' knowledge, there exists not yet an integrated platform to combine this approach with the speciation calculations and density corrections required to describe a solvent extraction system. Consequently, the state-of-the-art favours semi-empirical, single-framework activity models that balance chemical soundness with adjustable interaction parameters, offering the broadest applicability and best predictive capability for designing next-generation hydrometallurgical processes.

In this paper, we describe a thermodynamic model based on the OLI-MSE framework to calculate the equilibria of solvent extraction systems for H_2SO_4, HCl, and MSA by an organic phase containing TEHA, 1-octanol, and their mixtures, undiluted or diluted in aliphatic diluents. The construction of the model requires an analysis of the liquid–liquid equilibrium data obtained from the literature and new experiments, and the extraction mechanisms. Data on H_2SO_4 extraction from a feed with H_2SO_4 and $NiSO_4$ are used to validate the model.

2. Experimental

2.1. Chemicals

Hydrochloric acid solution (~37 wt%), sulphuric acid (95%), 1-octanol (99%), imidazole (99%), and *n*-dodecane (99%) were purchased from Fisher Scientific (Geel, Belgium). Methanesulphonic acid (MSA, 99.5%) was purchased from Carl Roth (Karlsruhe, Germany). Tris(2-ethylhexyl)amine (99.8%) was purchased from Merck Life Science (Darmstadt, Germany). Potassium hydroxide solution (0.1 mol L^{-1}), nitric acid solution (>65%), and propan-2-ol (>99%) were purchased from AnalytiChem (Zedelgem, Belgium). Disodium oxalate (>99.8%) was purchased from VWR Chemicals (Leuven, Belgium). Water was always of ultrapure quality, deionised to a conductivity of less than 0.055 μS cm^{-1} (298.15 K) with a Merck Millipore Milli-Q Reference A+ system. All chemicals were used as received, without any further purification.

2.2. Solvent extraction experiments

Solvent extraction experiments were performed by contacting 5 mL of aqueous feed with 5 mL of organic phase in 20 mL glass vials for 30 min at 200 rpm and 25 °C in a Thermoshake THL 500/1 from Gerhardt. Shaking was carried out for 30 minutes to ensure that the equilibrium condition was attained; these systems typically reach equilibrium within 2 to 5 minutes.[41,42] After shaking, the glass vials were centrifuged, and the phases were physically separated. Aqueous feed solutions were prepared by diluting a known mass of acid to a certain volume. The acid concentration ranges were selected to cover the typical conditions for acid recovery that are met in hydrometallurgical processes.[4] Similarly, the organic phase was prepared by weighing a defined mass of TEHA and 1-octanol, and diluting with *n*-dodecane whenever necessary.

Acid concentrations in the aqueous feed, the aqueous solution after extraction, and the organic solution after extraction were determined by titration with 0.1 mol L^{-1} KOH using a METTLER TOLEDO T5 Excellence autotitrator. A DGi111-SC pH electrode (METTLER TOLEDO) was used for the equivalence point determination in aqueous solutions, and a DGi113-SC pH electrode (METTLER TOLEDO) was used for analysing the organic phase. Propan-2-ol was used as the medium for the titration of the organic solution, as both the organic solution and the titrant were soluble in this solvent, based on preliminary tests. Sodium oxalate was added to the aqueous solutions to prevent Ni(II) hydrolysis. The water content in the organic phase at equilibrium was determined by titration using a volumetric V30S Karl Fischer titrator (METTLER TOLEDO) by direct addition to the reactor. Imidazole was added to the reactor to maintain an optimal pH. The density of the organic phase was measured using a DMA 4500 M density meter (Anton Paar). Volume changes and the connected organic to aqueous volume ratio at equilibrium $(O/A)_e$ were either determined visually in a graduated cylinder or through calculation from the complete composition of the organic phase and its density. Fourier-transform infrared (FTIR) spectra on undiluted TEHA loaded with different amounts of MSA through solvent extraction were recorded in ATR mode on a Bruker Vertex 70 FTIR spectrometer, equipped with a platinum ATR module and a diamond sample crystal at a resolution of 1 cm^{-1}.

The *distribution ratio* (D) of an acid was calculated by dividing its measured molarity in the organic phase ($[HX]_o$) by that in the aqueous phase ($[HX]_a$). From this value, the *Gibbs free energy of transfer* (ΔG_{TR}) for an acid was calculated as follows:

$$\Delta G_{TR} = \frac{-R \cdot T \cdot \ln(D)}{1000} \quad (1)$$

ΔG_{TR} is expressed in kJ mol^{-1}, with R being the universal gas constant (8.314 J mol^{-1} K^{-1}) and T the temperature in Kelvin. Also, the *extraction efficiency* (% E) of an acid was calculated as follows:

$$\%E = 100 \cdot \frac{[HX]_o \cdot V_o}{n_{HX,f}} \quad (2)$$

with V_o being the volume of the organic phase at equilibrium and $n_{HX,f}$ being the number of moles of HX in the feed. The *percentage loading* (% L) of the extractant was expressed as:

$$\%L = 100 \cdot \frac{[HX]_o \cdot V_o}{n_{TEHA,f}} \quad (3)$$

based on the hypothesis that the acid : TEHA stoichiometry in the extracted species is 1 (*vide infra*).

3. Results and discussion

3.1 Experimental data

Literature data have been extended with new experiments to build a dataset used to construct the thermodynamic model.[14,15,41–48] An overview of the experimental conditions covered by the literature data and new experimental data is presented in the SI (SI, Table S1). These data comprise feed solutions containing only water or aqueous solutions of H_2SO_4 (0.04–14 mol L^{-1}), HCl (0.08–9.4 mol L^{-1}), or MSA (0.06–10.2 mol L^{-1}). The organic phase is either TEHA or 1-octanol, or mixtures of these two extractants with or without an aliphatic diluent. The initial organic-to-aqueous volumetric phase ratio (O/A) was almost always equal to 1.0, except when stated otherwise in SI Table S1. The data contain one or more of the following equilibrium properties, measured between 25 and 80 °C: acid extraction, water–extractant mutual solubility, volume change, organic phase density, and pH.

New experiments were needed to fill gaps in the literature dataset, specifically for undiluted 1-octanol and undiluted TEHA systems, data on organic phase water uptake, and volume changes. The experimental details and all measured equilibrium properties are provided in SI Table S2.

For organic phases containing only 1-octanol, data were limited to systems with H_2SO_4. Therefore, the extraction, density of the organic phase, and volume changes of H_2SO_4, HCl, and MSA systems with 1-octanol were determined at equilibrium (Fig. 1). D values are similar for all three acids, but MSA extraction efficiency is significantly higher at high MSA concentrations due to the larger phase ratio at equilibrium, $(O/A)_e$. More coextraction of water most likely leads to this larger $(O/A)_e$ and results in the formation of a single phase at 10 mol L^{-1} MSA. Despite the lower $(O/A)_e$ and reduced water uptake in the H_2SO_4 system, the organic phases loaded with MSA and H_2SO_4 exhibit similar densities. This can be attributed to the inherently higher density of H_2SO_4 solutions.

The behaviour of systems with undiluted TEHA as the organic phase was investigated experimentally, as only a single data point with this condition and an MSA feed solution was found in the literature.[14] The extraction of MSA by undiluted TEHA was studied by varying the (feed) MSA concentration ($[MSA]_f$) at room temperature, while also some data were collected for H_2SO_4 and HCl (Fig. 2). The H_2SO_4

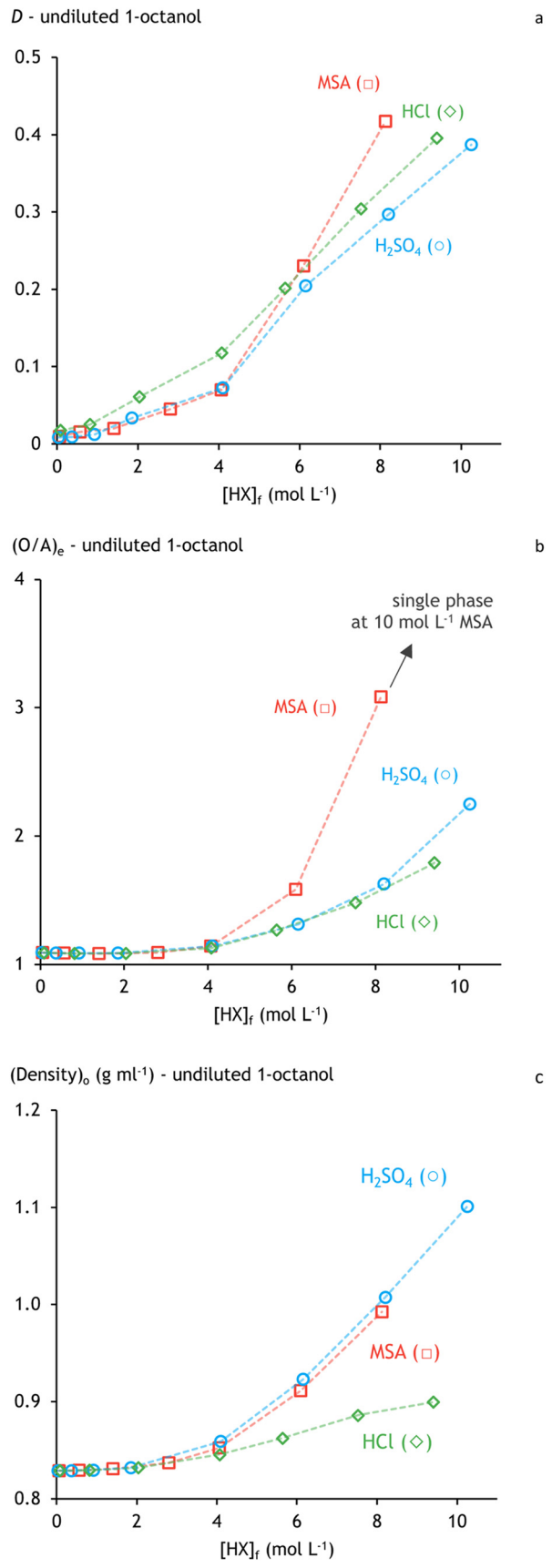

Fig. 1 Solvent extraction data of H_2SO_4, HCl, and MSA – undiluted 1-octanol systems at 25 °C. Distribution ratios (a), volume changes (b), and organic phase densities (c) are shown.

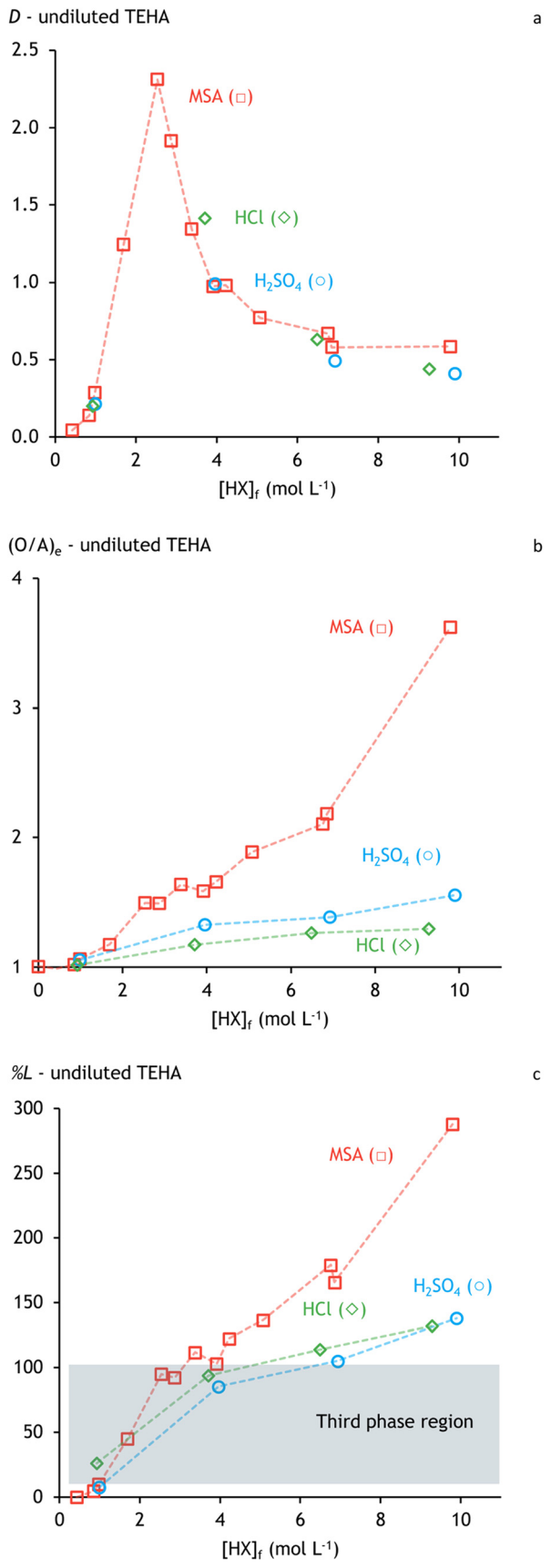

Fig. 2 Solvent extraction data of H_2SO_4, HCl, and MSA – TEHA systems at 25 °C. Distribution ratios (a), volume changes (b), and extractant loadings (c) are shown.

and HCl systems were studied in less detail, as the thermodynamic model can interpolate based on the combined data of all three systems due to the similar extraction mechanism (see below).

Third-phase formation was encountered in all samples with % E between 5 and 100. Further analysis showed that the top organic phase was lean in water and acid. In contrast, the bottom organic phase was richer in water content and fully loaded with acid, indicating that the extracted acid-TEHA complex has a low solubility in free TEHA. The average properties of the total organic phase under these conditions were determined by taking the volume-weighted average of the measurements in the separate organic phases. D increases with increasing $[HX]_f$ until 100% organic loading is reached. The extractant loading still increases above 100% at higher $[HX]_f$, but the corresponding decrease in D indicates that this is less favourable. Similar to the 1-octanol system, the $(O/A)_e$ increases much more in MSA systems compared to H_2SO_4 and HCl systems. This results in a higher % E for MSA, despite the similar D values for the extraction of all acids by TEHA. This larger increase in $(O/A)_e$ when MSA gets extracted coincides with a larger uptake of water by the organic phase (see SI, Table S2).

Dilution of TEHA can be useful to fine-tune acid recovery and reduce viscosity. In industry, aliphatic diluents are preferred over aromatic diluents because they are safer, have a lower environmental impact, and result in relatively higher extraction efficiencies.[49] Only limited extraction efficiency data are available in the literature, covering TEHA concentrations between 9 and 43 vol% and lacking key experimental details.[14,46,47] New experiments were performed to investigate the system at higher TEHA concentrations and under selected conditions from previous studies to complete and validate the existing dataset.

n-Dodecane was chosen as a model diluent for a large group of aliphatic diluents, as they all have a similar effect on the solvent extraction equilibrium. Aliphatic diluents are often ineffective in solvating the extracted complex. For the extraction of mineral acids by TEHA, this also leads to third-phase formation between 5 and 100% extractant loading (Fig. 3). The order of % E is HCl > H_2SO_4 > MSA in the region below 3 mol L^{-1} acid in the feed. Only the aqueous acid concentration was measured for this set of experiments due to third-phase formation in several samples. The average acid concentration in the organic phase and the percentage extraction were determined based on the mass balance, with volume changes taken into account.

Adding 1-octanol can enhance the acid – TEHA solvent extraction system by reducing viscosity, improving extraction efficiency, and preventing third-phase formation. While extensive literature exists on TEHA, 1-octanol, and *n*-dodecane systems, these reports focus only on the acid extraction itself.[14,15,42,46–48] A limited number of new experiments with TEHA and 1-octanol in the organic phase were performed to investigate acid extraction, water uptake by the organic phase, volume changes, organic phase density,

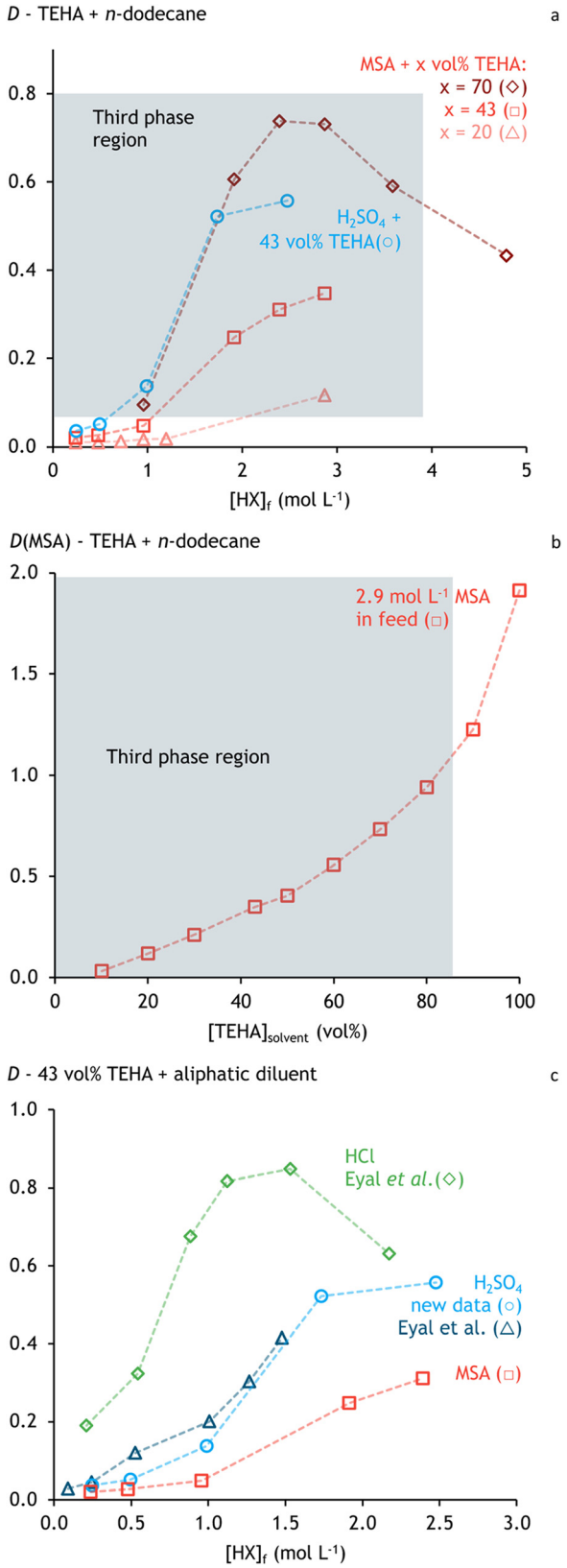

Fig. 3 Solvent extraction data of H_2SO_4, HCl, and MSA – TEHA + dodecane systems at 25 °C. Graph c compares this to literature data from Eyal *et al.*[46] Distribution ratios are shown for three TEHA concentrations with varying H_2SO_4 concentrations in the feed (a), and with varying initial TEHA concentrations in the solvent (b). (c) Compares the extraction of HCl, H_2SO_4, MSA by 43 vol% TEHA.

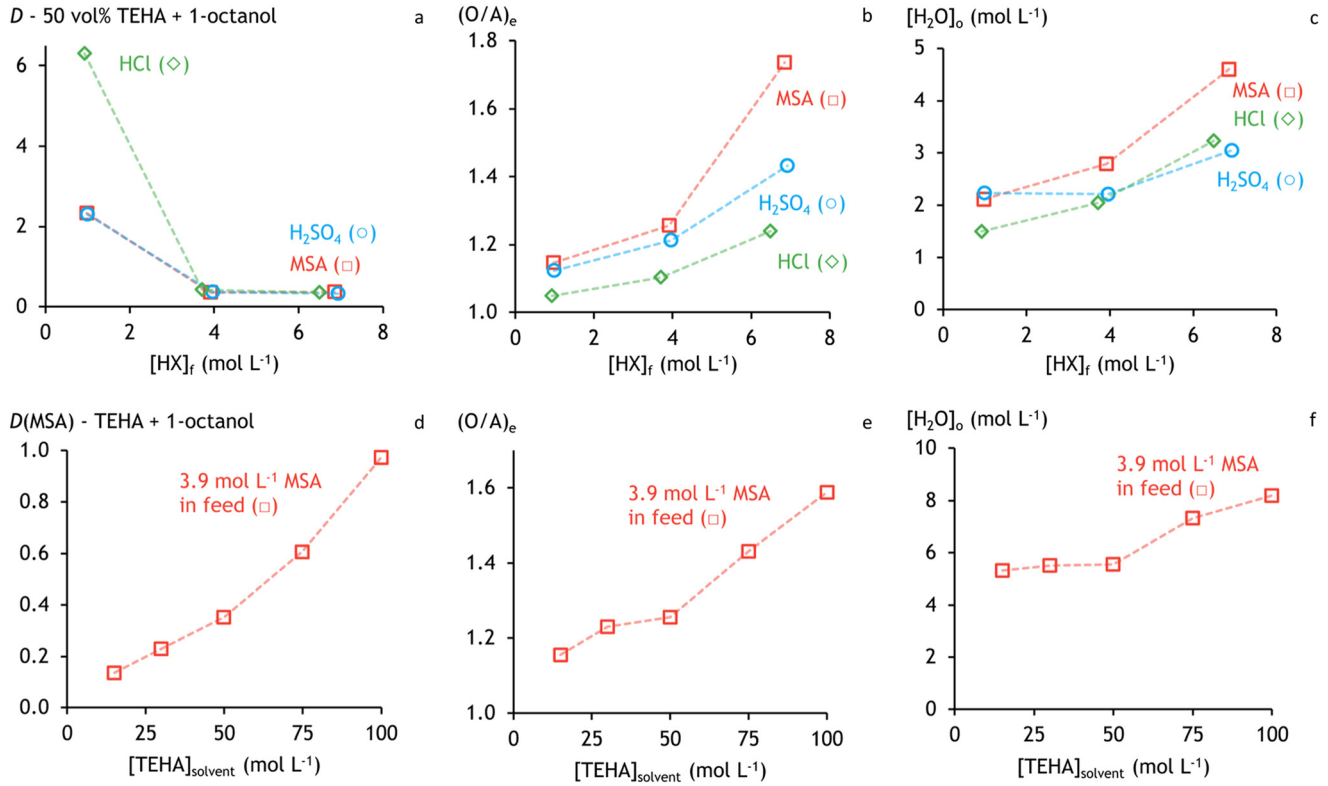

Fig. 4 Solvent extraction data of H_2SO_4, HCl, and MSA – TEHA + 1-octanol systems at 25 °C. Systems depicted in a to c contain 50 vol% TEHA in 1-octanol, and in d to f contain a variable amount of TEHA in 1-octanol. Distribution ratios (a and d), volume changes (b and e), and water uptake by the solvent (c and f) are shown.

and aqueous equilibrium pH in MSA, H_2SO_4, and HCl systems. This results in a more complete picture of the equilibrium (Fig. 4).

No third-phase formation was observed at the investigated TEHA concentration in 1-octanol. HCl extraction by 50 vol% TEHA + 1-octanol is significantly more efficient than H_2SO_4 or MSA extraction at low acid concentrations. The extraction of H_2SO_4 and MSA is very similar in terms of D and % E below 4 mol L^{-1} acid in the feed, but % E of MSA will be higher than that of H_2SO_4 and HCl above 4 mol L^{-1} acid due to a larger volume increase of the organic phase. The similar extraction efficiency of MSA and H_2SO_4 at lower acid concentrations can also be inferred from the literature by comparing data from Haghshenas *et al.*, Eyal *et al.*, and the thesis of Kwok *et al.*[14,42,46] Only a few data points with TEHA and 1-octanol could be compared, specifically around 43 vol% TEHA and 1.0 mol L^{-1} acid in the feed. Haghshenas *et al.* and Eyal *et al.* reported % $E(H_2SO_4)$ of 68 and 70% respectively. Kwok *et al.*, working exclusively with MSA, observed a % E of 66 at 40 vol% TEHA and 70 at 50 vol% TEHA.

The amount of water in the organic phase ($[H_2O]_o$) generally increases with increasing acid concentration in the feed (Fig. 4c). The interpretation of the relation between $[H_2O]_o$ and acid extraction is not straightforward, indicating that there is no evidence for the formation of one complex with a fixed acid-TEHA-H_2O stoichiometry in mixed TEHA – 1-octanol systems. Non-linearity is also observed for $[H_2O]_o$ *versus* TEHA concentration in 1-octanol at 3.9 mol L^{-1} MSA_f (Fig. 4f). Here, the $[H_2O]_o$ stays almost constant above an equimolar ratio of $[MSA]_o$ and $[TEHA]_o$, but increases at the equimolar ratio with increasing $[TEHA]_o$. The non-linear trends might even indicate a change in solvent extraction mechanism, but too few data were available to draw any decisive conclusions at the time of our study. Therefore, a more detailed analysis of the extraction mechanism, based on Fourier-transform infrared (FTIR) spectroscopy and a literature analysis, was performed.

3.2. Solvent extraction mechanism

First, the solvent extraction mechanism for 1-octanol is discussed, followed by TEHA, and finally the synergistic TEHA + 1-octanol system. This approach is also followed for the part on the model development. The extraction of mineral acids by 1-octanol is governed by a partial replacement of the hydration sphere of the acid by 1-octanol. This process can be described as a non-reactive extraction, as no covalent bonds are broken or formed. Since 1-octanol is slightly polar and can form hydrogen bonds, both molecular and dissociated acid could be stabilised in the organic phase. Thus, it is assumed that the acid dissociation constant is not negligible in the organic phase. Gromov *et al.* observed a significant decrease in extraction efficiency for 6.0 mol L^{-1} H_2SO_4 by 1-octanol, indicating the exothermic nature of the extraction.[41] A similar effect is expected for the extraction of MSA and HCl, since the extraction mechanisms are the same.

TEHA is a rather alkaline branched ternary amine with a predicted pK_a of 9.3 ± 0.5.[50] The lack of an experimental pK_a value likely stems from TEHA's poor solubility in water. TOA is the most similar extractant to TEHA. They only differ in the branching of the alkyl chain, resulting in a slightly lower basicity for TEHA due to steric hindrance. TEHA can accept a proton on its nitrogen lone pair and solvate the conjugate base to extract acid:

$$HX_a + TEHA_o \rightleftharpoons (TEHAH^+)(X^-)_o \quad (4)$$

Here, HX_a represents an acid in the aqueous phase. This can be either in the protonated form or a hydrated proton and its conjugated base. This mechanism limits the extraction of an acid to a 1:1 stoichiometric ratio with TEHA. Literature data and experimental data presented above indicate that more acid can be distributed to the organic phase, necessitating a second extraction mechanism. It is assumed that $(TEHAH^+)(X^-)_o$ and some coextracted water can stabilise additional molecular acid in the organic phase through weak interactions:

$$HX_a \rightleftharpoons HX_o \quad (5)$$

The protonation of TOA is confirmed in the literature by FTIR analysis, but no spectra are available for TEHA.[12,15] FTIR spectroscopy was performed on undiluted TEHA loaded with MSA to study both proposed extraction mechanisms for TEHA (Fig. 5).

MSA vibrations are most clearly visible in the FTIR spectra, with key peaks between 1350 cm^{-1} and 1000 cm^{-1} (Fig. 5b). The SO_3 symmetric stretch appears at 1172–1165 cm^{-1} and 1115 cm^{-1}, compared to 1122 cm^{-1} in pure liquid MSA.[51] Weakened hydrogen bonding due to the protonation of TEHA most likely leads to the shift to higher wavenumbers. Thus, the signal at 1172–1165 cm^{-1} indicates the formation of a $(TEHAH^+)(OSO_2CH_3^-)$ complex as proposed by eqn (4). The direct environment of SO_3 from the signal around 1115 cm^{-1} should more closely resemble that of MSA in its pure liquid state (1122 cm^{-1}), indicating stronger H-OSO_2CH_3 interactions. This may involve direct bonding or bridging *via* coextracted water $(H^+\text{-}(O_2H)_x\text{-}OSO_2CH_3^-)$, and corresponds to the second part of the extraction mechanism (eqn (5)) that governs acid extraction beyond an equimolar MSA:TEHA ratio.

For further analysis, the spectra in the spectral region between 1300 and 1100 cm^{-1} were deconvoluted with a Lorentzian profile (Fig. 6). The area of the signal around 1169 cm^{-1} remains almost constant with increasing loading compared to the area of the signal at 9% *L*, confirming the stable concentration of the protonated TEHA complex (eqn (4)). Meanwhile, the growing signal at 1115 cm^{-1} closely follows the increase in free MSA, supporting its role in eqn (5). Here, free MSA indicates the MSA concentration above a 1:1 stoichiometry with TEHA.

Other signals from MSA include the S–O–H in-plane bend and the SO_3 asymmetric stretch. The S–O–H bend shifts from 1166 cm^{-1} in pure MSA to 1219 cm^{-1} in the $(TEHAH^+)(OSO_2CH_3^-)$, while the SO_3 symmetric stretch shifts slightly above 1325 cm^{-1}.[51] The signal around 1100 cm^{-1} on the spectrum with % *L* = 1 corresponds to the C–N stretch of TEHA, based on the similar location of the C–N stretch in TOA.[12,15] This signal shifts to 1042 cm^{-1} upon protonation of the N lone pair. Since spectra were recorded at either negligible % *L* or % *L* > 100 due to third-phase formation, only the original or shifted signal was observed. The relatively constant intensity of the shifted signal above 100% *L* suggests no further TEHA protonation, consistent with the analysis above.

The H_2O:MSA ratio in the organic phase above 100% *L* is 2.03 ± 0.08, indicating coextraction of two water molecules per additional extracted MSA above 100% *L*. At non-zero % *L*,

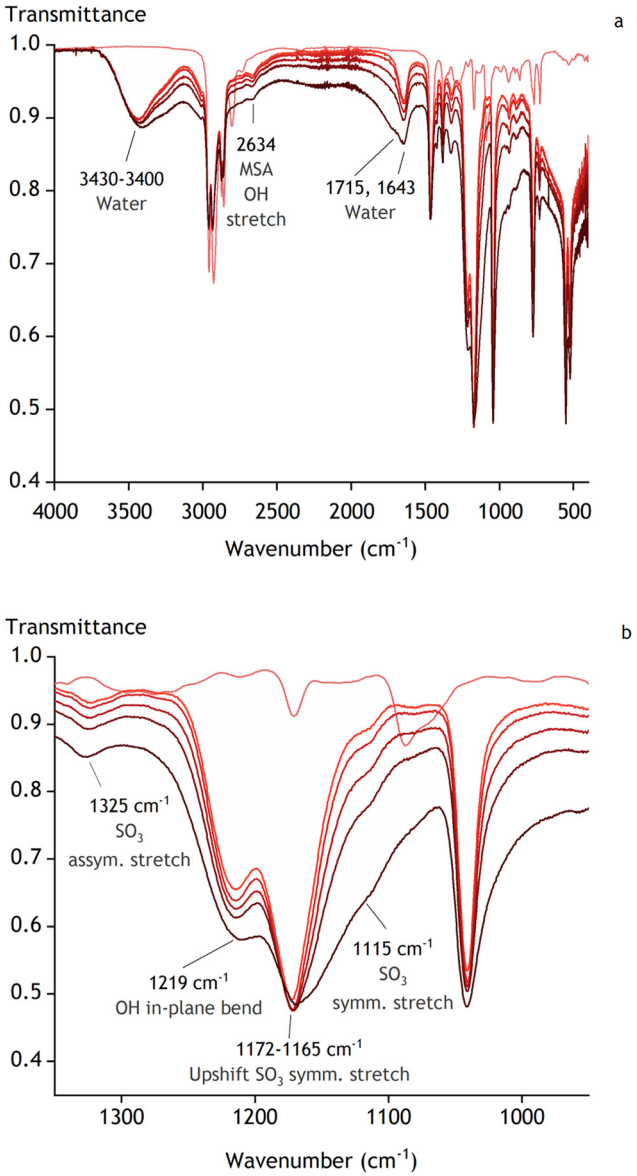

Fig. 5 FTIR spectra of TEHA loaded with increasing MSA concentrations from light red to black. 1% *L* and 0.003 mol L^{-1} H_2O (—), 95% *L* (—), 112% *L* and 4.2 mol L^{-1} H_2O (—), 122% *L* and 4.3 mol L^{-1} H_2O (—), 137% *L* and 5.3 mol L^{-1} H_2O (—), 179% *L* and 6.3 mol L^{-1} H_2O (—). (a) Shows the full spectra, while (b) displays a zoom on the most relevant region for MSA vibrations.

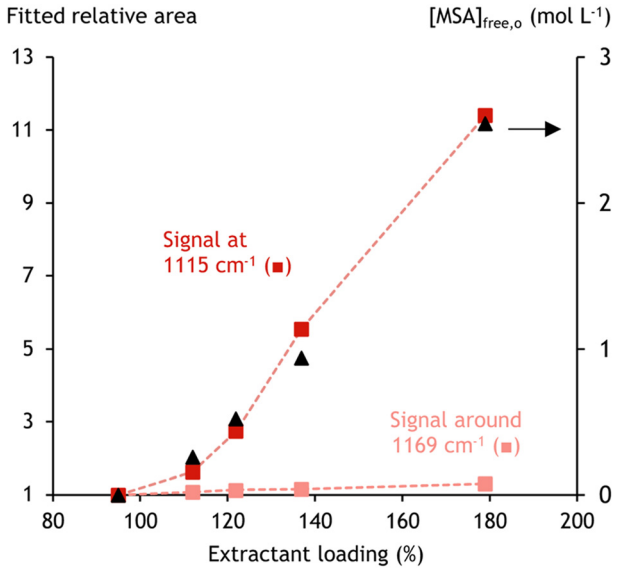

Fig. 6 Areas of deconvoluted FTIR peaks relative to their area at 95% *L* (■), compared to free acid concentration in the organic phase based on eqn (4) and (5) (▲).

a H_2O signal at 1643 cm^{-1} remains constant with increasing % *L* above 100, while a second H_2O signal emerges with increasing loading above 100% *L*. These 2 distinct signals show that water is present in the organic phase in two distinct coordination environments. The signal at 1643 cm^{-1} probably corresponds to H_2O involved in the reactive extraction of MSA (eqn (4)), while the second signal reflects water associated with excess MSA extraction (eqn (5)). The latter H_2O molecules are likely part of a solvent-shared ion pair as presented above (H^+-$(O_2H)_x$-$OSO_2CH_3^-$). A H_2O signal can also be found around 3400 cm^{-1}, and this seems to split towards lower wavenumbers. Most likely, both vibrations of a protonated amine (N–H) bond and water contribute to this shoulder, making further analysis more difficult.[52]

The HCl > H_2SO_4 > MSA extraction trend with diluted TEHA (Fig. 3) appears to contradict the more efficient extraction of 4 mol L^{-1} or more MSA by undiluted TEHA (Fig. 2), but this is explained by differences in % *L*. Fig. 3 reflects conditions below a 1 : 1 acid : TEHA molar ratio, where extraction is driven by preferential acid–extractant interactions. Above 100% *L*, these interactions become less relevant, and the higher $(O/A)_e$ from increased water uptake in MSA-loaded organic phases becomes the dominant factor.

When 1-octanol is added, the extraction mechanism remains unchanged, but 1-octanol acts as a modifier and a synergist. It prevents third-phase formation below 100% *L* by solvating the $(TEHAH^+)(X^-)$ complex, as seen by the absence of third-phase formation in Fig. 4 while % *L* varies between 58.5 and 230 (SI Table S2). The literature also shows improved H_2SO_4 extraction when part of the aliphatic diluent is replaced by 1-octanol in systems where % *L* is below 100.[15,42,46,53] The combined TEHA + 1-octanol system shows a synergistic effect:

$$(D)_{x(\mathrm{TEHA})+y(1\text{–octanol})} > (D)_{x(\mathrm{TEHA})} + (D)_{y(1\text{–octanol})} \quad (6)$$

This synergy is also evident for MSA. While SI Table S2 lacks data that directly fits eqn (6), stronger synergy was observed with 100 vol% of each extractant. For example, *D*(MSA) for 1.0 mol L^{-1} MSA with 50 vol% TEHA and 1-octanol is 2.3, compared to 0.28 for undiluted TEHA and 0.016–0.020 for undiluted 1-octanol.[14] Similarly, *D*(HCl) for 0.9 mol L^{-1} HCl by 50 vol% TEHA and 1-octanol is 6.3, *versus* 1.8 for undiluted TEHA and 0.025 for undiluted 1-octanol.

The reduction of third-phase formation and synergy when adding 1-octanol to systems containing TEHA probably relate to the tendency of ternary amines to form reverse micelles in solvent extraction systems.[54] TOA and other ternary amines readily form reverse micelles, especially when the polarity of the head is increased by protonation through acid extraction or by extraction of metal–ligand ion pairs.[54,55] TEHA's branched alkyl chains close to its polar head hinder micelle formation compared to linear-chain amines. No evidence for reverse micelles was found for TEHA at 0.2 mol L^{-1} amine in *n*-dodecane and 5 vol% 1-octanol, while systems with linear or differently branched amines did show reverse micelle formation.[55] Third-phase formation in the system studied by Guerinoni *et al.* occurred only at TEHA concentrations exceeding 1.17 mol L^{-1} in *n*-dodecane (>50 vol%).[54] For TOA, third-phase formation was observed at 0.1 mol L^{-1}, matching its critical aggregation concentration (CAC) of 0.08 mol L^{-1} in a similar system. Although the limit for third-phase formation is not necessarily linked to the CAC, its match for TOA suggests that the CAC for TEHA is around 50 vol% at 0.1 mol L^{-1} H_2SO_4.

The current study uses higher TEHA and acid concentrations, increasing the likelihood of exceeding the CAC. This is supported by the significantly higher acid extraction and water uptake compared to a system from Lu *et al.* with 0.1 mol L^{-1} $H_2SO_{4,f}$ and 0.2 mol L^{-1} TEHA in *n*-dodecane with 5 vol% 1-octanol.[55] TEHA's higher CAC may also explain the opposite extraction trends with increasing $[H_2SO_4]_f$.[15] TOA shows decreasing % *E* due to loading effects, while TEHA shows increasing % *E* up to 1.5 mol L^{-1} $H_2SO_{4,f}$, possibly due to CAC crossing. In both cases, % *L* remains significant but below 100.

The relations between the compound type, concentration, reverse micelle formation, third-phase formation, and synergistic effects are complex.[56] Due to TEHA's relatively high CAC, detailed studies on its micelle behaviour are lacking.[54,57,58] Consequently, insights from TOA and other amine-based systems have been extrapolated here to TEHA systems. 1-Octanol acts as a cosolvent, penetrating only the outer shell of the TOA reverse micelles. This inhibits reverse micelle coalescence and prevents third-phase formation.[58] A similar mechanism likely applies to TEHA. Synergistic effects in TEHA – 1-octanol systems may arise from two mechanisms.[59,60] (1) 1-Octanol's linear chain offers less steric hindrance, solvating $(TEHAH^+)(X^-)$ more effectively than TEHA. (2) 1-Octanol may stabilise reverse micelles large enough to accommodate acid and water by reducing the packing parameter of the system.[61]

TEHA's branched chains near its polar head significantly increase its packing parameter compared to TOA, hindering the formation of sufficiently large reverse micelles.[54] Both mechanisms suggest favourable interactions among ($TEHAH^+$) (X^-), TEHA, and 1-octanol, but further research is needed to clarify their individual contributions.

3.3. Thermodynamic model development

The aqueous and solid-state species, thermodynamic values, and interaction parameters of MSA, H_2SO_4, and HCl are already available in the general MSE database of OLI Systems, Inc.[36,37,62] This aqueous phase chemistry is the first requirement for calculating a solvent extraction equilibrium. An accurate description of the chemistry in the organic phase and its interaction with the aqueous phase is the second, but the general MSE database of OLI Systems, Inc. only covers the chemistry of *n*-dodecane. 1-Octanol, TEHA, and its conjugated acid ($TEHAH^+$) were added to a new OLI-MSE database that can be used on top of the general database, and their solution state properties at the standard state of infinite dilution in water were estimated. Literature and experimental data (SI Tables S1 and S2) were used to optimise the standard state thermodynamic values along with the interaction parameters through fitting procedures.

The solvent extraction database was constructed in several stages. In each stage, only the thermodynamic values and interaction parameters that were newly introduced were optimised. The process began by modelling the extraction of acids by 1-octanol. Then, the acid – undiluted TEHA chemistry was modelled, followed by a dilution of TEHA with an aliphatic diluent. Finally, the data of synergistic systems were added to the fitting procedure. This stepwise approach enhances the model's reliability and reduces the risk of overfitting by ensuring that the optimised parameters are directly aligned with the experimental data they influence.

1-Octanol does not undergo any chemical reaction in the solvent extraction systems presented here. Only relevant are the mutual solubility of 1-octanol and water, the liquid density, and the weak interaction of 1-octanol with MSA, H_2SO_4, and HCl. An estimation or approximation of its standard state thermodynamic values thus suffices and can be found in Table 1. These values were not further optimised during the fitting procedure. The *standard state Gibbs free energy of formation* (ΔG_f^0) of 1-octanol infinitely diluted in water could not be found in the literature; instead, that of the ideal gas was used.[63] The *standard state enthalpy of formation* (ΔH_f^0) was added as the average of four values found in the literature.[64–67] The *standard state heat capacity* (c_p) was determined as the average of the two most recent values found in the literature.[68,69] The *standard state entropy* (S^0) was calculated using the following formula:

$$\Delta G_f^0 = \Delta H_f^0 - T\left(S^0 - \sum_i \nu_i S_i^0\right) \quad (7)$$

where i represents the ith element of 1-octanol in its standard state and ν_i is its stoichiometry of that element in 1-octanol.

The UNIQUAC equations are used in the OLI-MSE framework to represent deviations from ideality due to short-range chemical interactions.[36] These deviations represent the weak interactions between neutral molecules that govern the mutual solubility of water and 1-octanol. The entropic contribution to the UNIQUAC equations requires a size and surface parameter.[70] These were estimated based on the UNIFAC method from Hansen *et al.*[71] Finally, the standard state molar volume (V_m^0) was calculated based on the pure liquid density at 25 °C, while temperature corrections were also added to represent the density between 5 °C and 85 °C.[72] These one-species-specific values can also be found in Table 1.

The short-range binary interaction parameters (a_{ij} and a_{ji}) were fitted to data of the mutual solubility with water.[43,44] The variations with temperature were introduced in the model by a temperature dependence on a_{ij} and a_{ji}, expressed in Kelvin:

$$a = a_0 + a_1 T + a_2 T^2 \quad (8)$$

Afterwards, new and literature data on ΔG_{TR}(acid), volume changes, organic phase density, and H_2O – 1-octanol mutual solubility were introduced for systems containing MSA, H_2SO_4, or HCl.[41] From these 112 data points, short-range binary interaction parameters between the protonated acid and 1-octanol and mid-range binary interaction parameters (b) between acid anions, H_3O^+, and 1-octanol were fitted. Despite limited data on full organic phase composition, organic phase density was calculated with acceptable accuracy, without using binary density parameters. Only temperature-dependent data for H_2SO extraction (25–70 °C) were available. To avoid overfitting, only a_1 was used for temperature corrections, and the values for a_1(MSA – 1-octanol) and a_1(HCl – 1-octanol) were set equal to a_1(H_2SO_4 – 1-octanol). For the mid-range interaction parameters, an

Table 1 Standard-state properties, molar volume (V_m), and UNIQUAC size (r) and surface (q) parameters in the thermodynamic model after optimisation with experimental data

Species	ΔG_f^0	ΔH_f^0	S^0	c_p^0	r	q	V_m
	kJ mol^{-1}	kJ mol^{-1}	J mol^{-1} K^{-1}	J mol^{-1} K^{-1}			L mol^{-1}
1-Octanol	−120.2	−428.7	289.5	304.8	6.622	5.828	0.1585
TEHA	321.0	−490.8	841.9	765.4	17.15	13.96	0.4329
$TEHAH^+$	268.3	−563.4	838.1	765.4	27.81	28.95	0.4329

ionic strength (I_x) correction (c_1, eqn (9)) and a temperature-dependent term (b_1, eqn (9)) were included, with $b_1(H_3O^+$ – 1-octanol) set equal to $b_1(HSO_4^-$ – 1-octanol). Table 2 contains an overview of all interaction parameters and their final values.

$$b = b_0 + b_1 T + \frac{b_2}{T} + c_0 \cdot \exp\left(-\sqrt{I_x + 0.01}\right) \quad (9)$$

ΔG_{TR} provides the most direct relation between solvent extraction and thermodynamics. Fig. 7a compares fitted and experimental ΔG_{TR} as a function of feed acid concentration, while Fig. 7b shows the calculated acid speciation in the organic phase. The latter is expressed as the ratio of protonated acid to total acid in the organic phase. The remaining extracted acid exists as contact- or solvent-shared ion pairs between H_3O^+ and the acid anion. Since this speciation cannot be directly measured and no literature data are available, the prediction may not fully reflect reality. Nevertheless, it results from a chemically-constrained, semi-empirical thermodynamic model that accurately reproduces acid extraction and water uptake.

A general overview of the thermodynamic model's performance, as indicated by quality-of-fit (QoF) plots, is presented in Fig. 8. These plots show the calculated *versus* the experimental datapoints, together with the ideal fit line (dashed grey) that represents a perfect fit of the experimental data by the thermodynamic model. A linear regression has been performed on the data.

The overlap of the confidence interval with the ideal fit line does not give any indication of a lack of fit for all QoF plots, except for that of $(density)_o$. This lack of fit stems from an underestimation of the $(density)_o$ in systems with H_2SO_4. For the $(O/A)_e$ QoF plot, the MSA data point around an experimental $(O/A)_e$ of 3.0 is excluded from the linear regression, as it deviates significantly from the other data points. The initial O/A ratio was always 1.0. Thus, only at a

Table 2 Optimised short- and mid-range binary interaction parameters in the OLI-MSE framework for the acid – TEHA – 1-octanol thermodynamic model

	Short-range[a]		Mid-range		
Species	a_{ij}	a_{ji}	b_{ij}[b]	c_{ij}[b]	d_{ij}[c]
H_2O – 1-octanol (0)	14 486	−10 453			
H_2O – 1-octanol (1)	−73.284	70.169			
H_2O – 1-octanol (2)	0.11035	−0.10192			
H_2SO_4 – 1-octanol (0)	−6260.9	−17 469			
H_2SO_4 – 1-octanol (1)	3.4568	23.8464			
CH_3SO_3H – 1-octanol (0)	−4209.6	−10 303			
CH_3SO_3H – 1-octanol (1)	3.4568	23.8464			
HCl – 1-octanol (0)	−891.83	−23 932			
HCl – 1-octanol (1)	3.4568	23.8464			
HSO_4^- – 1-octanol (1)			-6.8648×10^{-3}		
SO_4^{2-} – 1-octanol (1)			−0.12880		
$CH_3SO_3^-$ – 1-octanol (1)			-5.1612×10^{-3}		
Cl^- – 1-octanol (1)			3.3911×10^{-2}	-4.2000×10^{-2}	
H_3O^+ – 1-octanol (1)			-6.8648×10^{-3}		
OH^- – 1-octanol (1)			-6.8648×10^{-3}		
H_2O – TEHA (0)	2803.4	10 116			
H_2O – $TEHAH^+$ (0)	21.741	4619.3			
H_2SO_4 – TEHA (0)	−5632.7	2184.8	5.7162		
CH_3SO_3H – TEHA (0)	−4064.4	2184.8	6.9926		
HCl – TEHA (0)	−7388.2	2184.8	−14.261		
HSO_4^- – $TEHAH^+$ (0)					-4.6562×10^{-3}
$CH_3SO_3^-$ – $TEHAH^+$ (0)					-3.3903×10^{-2}
Cl^- – $TEHAH^+$ (0)					1.8526×10^{-2}
SO_4^{2-} – TEHA (2)			−7583.2		
H_3O^+ – TEHA (2)			−7583.2		
OH^- – TEHA (2)			−7583.2		
SO_4^{2-} – $TEHAH^+$ (2)			−7583.2		
H_3O^+ – $TEHAH^+$ (2)			−9583.2		
OH^- – $TEHAH^+$ (2)			−7583.2		
n-Dodecane – TEHA (0)	−2461.3	1953.3			
n-Dodecane – $TEHAH^+$ (0)	831.46	−546.00			
n-Dodecane – $CH_3SO_3^-$ (0)			9.6205	−9.2271	
n-Dodecane – HSO_4^- (0)			12.672	−12.107	
n-Dodecane – Cl^- (0)			14.583	−12.199	
1-Octanol – TEHA (0)	−3348.1	14613.0			
1-Octanol – $TEHAH^+$ (0)	−2076.7	1186.3	7.4452	−11.277	

[a] Short-range binary interaction parameters: $a = a_0 + a_1T + a_2T^2$. [b] Mid-range binary interaction parameters: $b = b_0 + b_1T + b_2/T + c_0 \cdot \exp(-\sqrt{I_x + 0.01})$. [c] Mid-range binary density parameter.

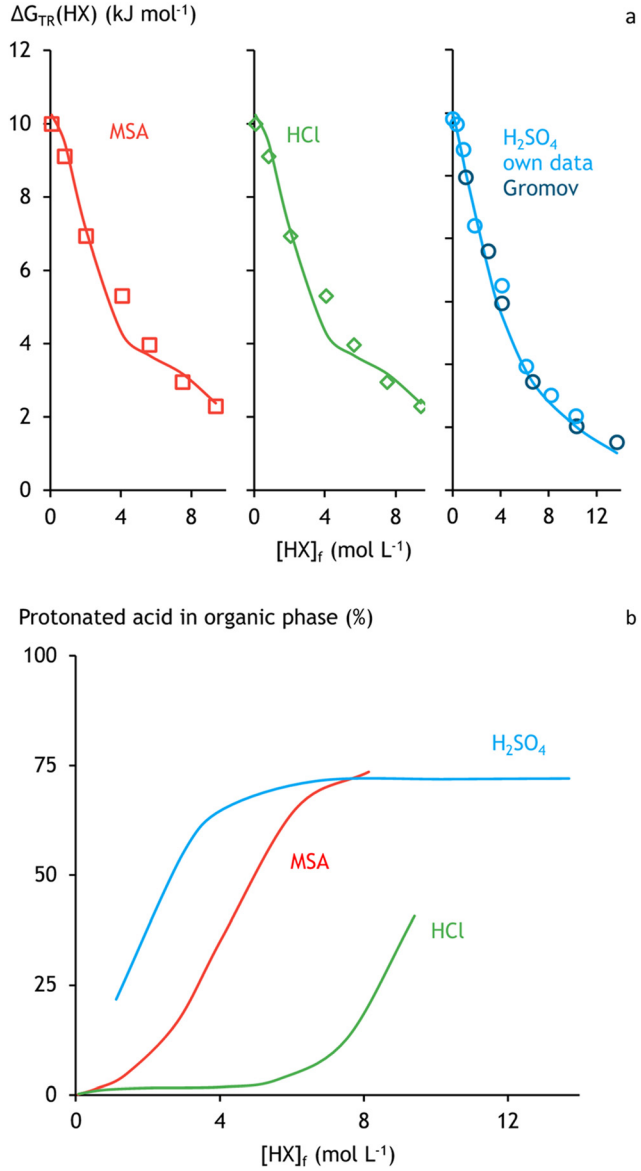

Fig. 7 (a) Fitted (lines) and experimental (markers) ΔG_{TR}, and (b) calculated acid speciation, in solvent extraction systems with undiluted 1-octanol.

substantial change in $(O/A)_e$, for systems containing a high concentration of MSA, an underestimation of the $(O/A)_e$ is calculated by the thermodynamic model.

The root mean square error (RMSE) and prediction interval indicate the expected error range of the thermodynamic model. With 95% confidence (2 times RMSE), the mean % E is predicted within ±5.1 of the experimental value. This non-zero error reflects limitations in the model, fitting inaccuracies, and experimental uncertainty. An experimental error of maximum ±10% E can be expected when combining both instrumental and random errors. As a result, the ±5.1% prediction error suggests that the thermodynamic model closely reflects reality. Similarly, the prediction error for $(O/A)_e$ is ±0.06 for experimental values in a range of 1.00–3.00. For $(density)_o$, this is ±0.02 g mL^{-1} for values ranging from 0.80 to 1.30 g mL^{-1}.

The mutual solubility QoF plot is more difficult to interpret, since it is shown in a log scale due to the 5 orders of magnitude difference in the solubility of 1-octanol in aqueous solution of H_2SO_4 and that of H_2O in 1-octanol. Also, the residuals are not normally distributed, as the deviations on the mutual solubility data of 1-octanol in $(H_2SO_4)_a$ are significantly larger. This is likely due to the challenges associated with accurately measuring such low concentrations of 1-octanol, especially considering that this solubility was not the primary focus of the original study.[41]

TEHA, TEHAH$^+$, and their standard state properties were added to the solvent extraction database following the same approach used for 1-octanol (Table 1). No direct thermodynamic data are available for TEHA and TEHAH$^+$, so these values are a rough estimate. ΔH_f^0, c_p^0, and S^0 were estimated using a Benson method.[73–75] ΔG_f^0 was calculated from the estimated ΔH_f^0 and S^0 values using eqn (7). The ΔG_f^0 value of TEHAH$^+$ was later fitted to reproduce the pK_a value of TEHA, which is estimated to be 9.3 ± 0.5 in water.[50] As a result of this approach, the thermodynamic values of TEHA and TEHAH$^+$ can only be used relative to each other, and these values should not be used in a broader context. V_m^0 was calculated from the density of TEHA at 25 °C (0.817 g mL^{-1}). TEHA's and TEHAH$^+$'s UNIQUAC size and surface parameters were estimated using a UNIFAC method.[71] The following chemical reaction was added to connect TEHA to TEHAH$^+$ in the thermodynamic model, for mass balance requirements:

$$TEHAH_a^+ + H_2O \rightleftharpoons TEHA_a + H_3O_a^+ \quad (10)$$

The OLI-MSE framework cannot handle more than two liquid phases. Thus, the third-phase formation observed below 100% L cannot be replicated by this thermodynamic model. This limitation is expected to have only a small effect on the performance of the thermodynamic model, as acid extraction between the aqueous phase and the organic phase still reaches equilibrium, and the average composition of the organic phase can be determined experimentally. In the model, this average composition is used to fit and validate equilibrium properties such as acid distribution, $[H_2O]_o$, and $(density)_o$. While third-phase formation may complicate phase separation in practical applications, it affects the thermodynamic equilibrium itself only to a minor extent.[76]

No data on the solubility of TEHA in water or aqueous acidic solutions could be found in the literature. Therefore, the solubility of TOA in water (1.1×10^{-7} mol L^{-1}) and trioctylmethyl ammonium chloride in 2 mol L^{-1} HCl (0.002 mol L^{-1}) were used to fit the binary short-range interaction parameters between TEHA and water, and TEHAH$^+$ and water, respectively.[77,78] To optimise these interaction parameters further, new data on the water uptake by undiluted TEHA in MSA, H_2SO_4, and HCl solvent extraction systems were used (SI Table S2). The thermodynamic model for the system with undiluted TEHA was finalised by fitting acid distribution data in the form of ΔG_{TR}, pH_e, $(density)_o$, $(O/A)_e$, and acid speciation in the organic phase according to

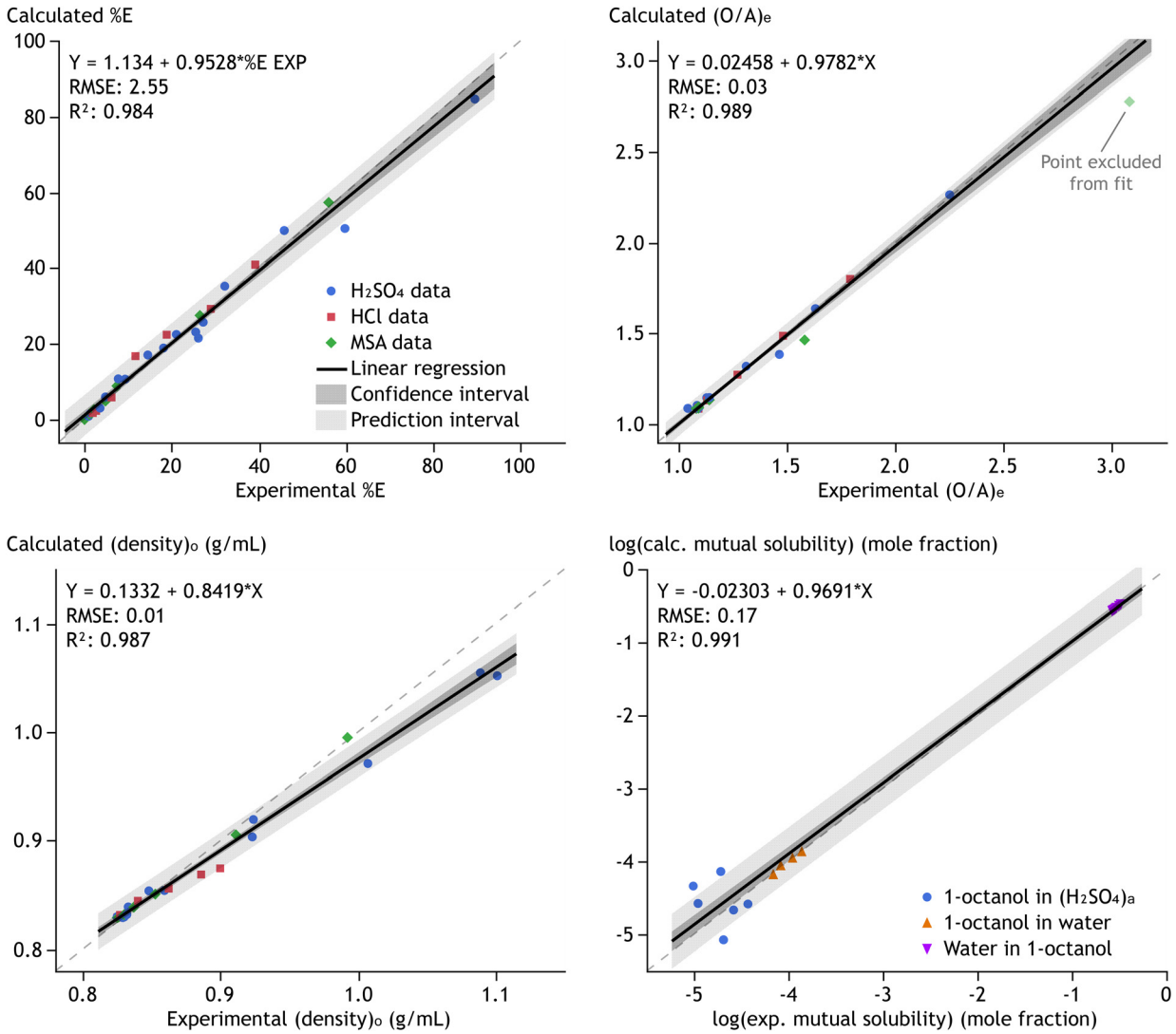

Fig. 8 Quality of fit graphs for 1-octanol data. Statistical intervals are given with 95% confidence. The dashed grey line represents the ideal fit.

the extraction mechanism presented above. 98 data points on systems with undiluted TEHA were used in total. This way, the effects of acid type and concentration at 25 °C were incorporated into the thermodynamic model by also optimising binary short-range and mid-range interaction parameters between molecular acid and $TEHAH^+$, and density parameters between acid anions and $TEHAH^+$ (Table 2). Large repulsive binary mid-range interaction parameters (b_2) were added for H_3O^+, OH^-, and SO_4^{2-} interactions with TEHA/$TEHAH^+$ to avoid the distribution of dissociated acid without reaction with TEHA and to limit the extraction of H_2SO_4 to the formation of $(TEHAH^+)(HSO_4^-)_o$ and $(H_2SO_4)_o$. This is customary practice in the OLI-MSE thermodynamic framework when no data are available on the very low distribution of a species between an aqueous phase and a solvent. The absence of SO_4^{2-} in the organic phase seems logical, as this higher-charged species is more difficult to stabilise than HSO_4^- in apolar media. Also, the short-range size and surface parameters of $TEHAH^+$ and its S^0 values

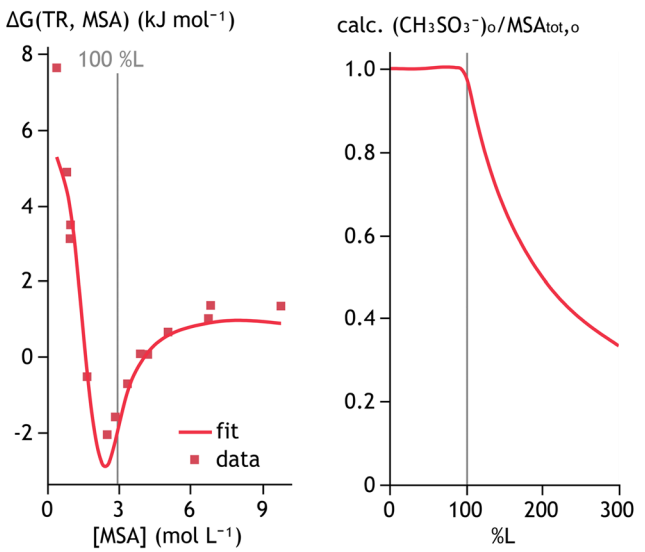

Fig. 9 Model fit of ΔG_{TR} and the calculated speciation of MSA extracted by undiluted TEHA.

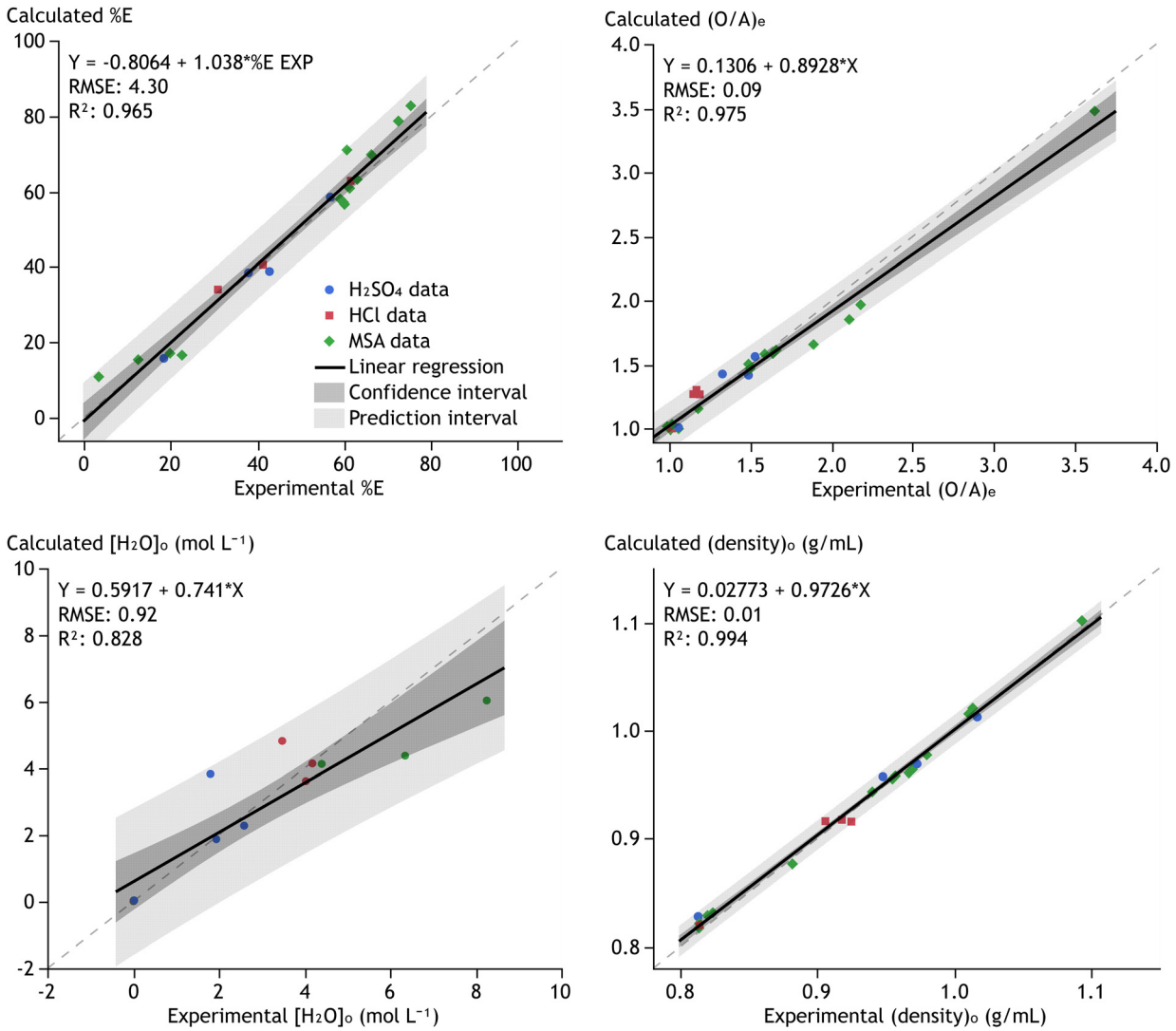

Fig. 10 Quality of fit graphs for undiluted TEHA data. Statistical intervals are given with 95% confidence. The dashed grey line represents the ideal fit.

were optimised to improve the performance of the thermodynamic model (Table 1).

The thermodynamic model can fit both ΔG_{TR} and the speciation change at 100% L of undiluted TEHA (Fig. 9). This clear match between model and experiments is not direct evidence for the proposed extraction mechanism (eqn (3) and (4)), as the mechanism is an input for building the model. Nevertheless, the proposed extraction mechanism is chemically feasible according to the model, on top of the experimental evidence provided for the extraction mechanism above.

The QoF graphs for the undiluted TEHA part of the thermodynamic model (Fig. 10) show no lack of fit for the % E and density. Most data points for $(O/A)_e$ show a good fit. Only at the highest $(O/A)_e$ data points in systems containing MSA, the thermodynamic model slightly underestimates the experimentally observed $(O/A)_e$ values. This is also observed for MSA – 1-octanol systems (Fig. 8). This discrepancy may be related to an underestimation of the water content in the organic phase under these conditions, but the limited number of data points for $[H_2O]_o$ limits the significance of this result.

A mean % E value can be calculated within an interval of ±8.6 (95% confidence) based on two times the RMSE (Fig. 10). This is again lower than the 10% E threshold, but higher than for the 1-octanol systems (Fig. 8). The error margin on $(O/A)_e$ of 0.18 indicates that the volume changes can be calculated within a relative error of ±20% for $(O/A)_e$ values of 1, which decreases further with increasing $(O/A)_e$ values. The underestimated values for the MSA system above an $(O/A)_e$ of 1.8 broaden the RMSE. Without these four data points, the RMSE lowers to 0.06. A very narrow prediction interval for $(density)_o$ is again observed, while that for $[H_2O]_o$ is rather broad. The experimental error on the water content determined by a Karl Fischer titration is expected to be quite significant, certainly due to the very high acidity of the samples. Although imidazole was used to neutralise this acidity, the residual effects may have compromised the

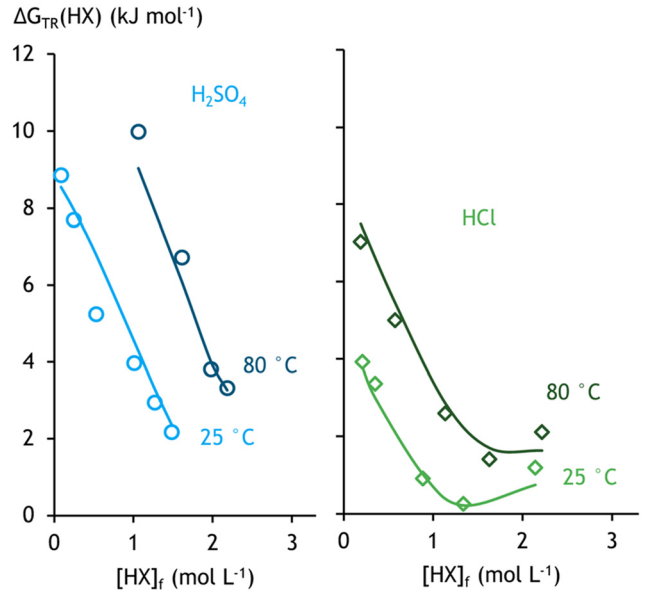

Fig. 11 Model fit of H_2SO_4 and HCl extraction by 43 vol% TEHA diluted in *n*-dodecane.[47]

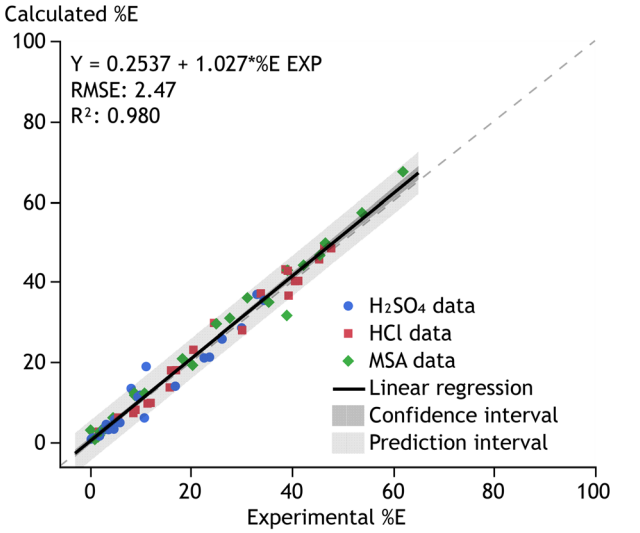

Fig. 12 Quality of fit graph for diluted TEHA data. Statistical intervals are given with 95% confidence. The dashed grey line represents the ideal fit.

accuracy of the measurements. This error likely explains much of the deviation observed in the $[H_2O]_o$ QoF plot. Based on the QoF plots, it does not seem that the larger deviations between calculated and measured $[H_2O]_o$ negatively impact the model accuracy regarding acid extraction.

74 data points from the literature and new experiments with TEHA and an aliphatic diluent (SI Table S1) were added to the fitting procedure. For the fitting procedure, *n*-dodecane was added as a model diluent for this group. The interaction parameters of TEHA and its protonated ion with the acid and acid ions were not further optimised. Only the temperature dependence was fitted by optimising the S^0 of $TEHAH^+$, since this was the first time that temperature-dependent data with TEHA were introduced.

The fit was further improved by introducing short-range binary interactions between *n*-dodecane and TEHA/$TEHAH^+$, and mid-range interaction parameters between *n*-dodecane and acid anions (Table 2). Both ionic strength independent (b_0, eqn (8)) and dependent (c_0, eqn (8)) contributions were required to fit the solubility of the acids in *n*-dodecane and the (de) stabilisation of the acids by *n*-dodecane with different concentrations of TEHA. Data on the solubility of mineral acids in *n*-dodecane are scarce, probably due to the difficulties in measuring such low solubilities in apolar solvents. Only one value for HCl (0.142 mol L^{-1}), the most soluble acid, could be found in the literature.[79] A fitted solubility of 0.196 mol L^{-1} was obtained when optimising this data point at 20 °C in equilibrium with HCl gas, together with the other data. Due to the lack of a value for the solubility of H_2SO_4 and MSA in *n*-dodecane, their calculated solubilities were kept below that of HCl.

Only acid extraction data were available for the systems with diluted TEHA. No volume changes were recorded in the literature, and they were too small to measure in the new experiments. Also, no $(density)_0$ and $[H_2O]_o$ data are available because little deviations from an ideal molar volume and a low water uptake are expected due to the presence of the apolar solvent. The current extension of the thermodynamic model builds further upon the model for undiluted TEHA, which is fitted to $(O/A)_e$, $(density)_0$, and $[H_2O]_o$ data.

The exothermic nature of acid extraction by amine extractants allows for improved stripping efficiencies of the acid by increasing the temperature.[14,47] This is especially interesting, as there are few tools to tweak the distribution for the extraction and stripping steps when the goal is to recover the acid directly rather than neutralising it first. Apart from the temperature effect, only dilution can be used to extract and strip significant or quantitative amounts of acid. The temperature effect is clearly visible for the extraction of HCl and H_2SO_4 by 43 vol% TEHA in *n*-dodecane, as shown in both the experimental data and the fitted curves (Fig. 11). This translates to an average decrease of 15 ± 4% *E*. No temperature-dependent data were available for MSA; however, the fitting results shown in Fig. 11 were obtained by optimising only $S^0(TEHAH^+)$. Since the thermodynamic model did not incorporate specific parameters for H_2SO_4 or HCl, there is no reason to expect that the temperature effect for MSA would be calculated less accurately.

At the 95% significance level, there is no indication of a lack of fit of % *E*, except at the highest % *E* values (Fig. 12). However, this lack of fit coincides with very few data points and is evident due to a very narrow confidence interval. Any calculated % *E* is still expected to be within ±4.9% *E* based on two times the RMSE values (95% confidence). This is a quite narrow prediction interval, compared to the tolerable error of ±10% *E* related to the plausible errors on the experimental data.

Finally, 239 data points for the synergistic system with both 1-octanol and TEHA were introduced to the fitting

procedure (SI Table S1). This includes both data for systems with and without an aliphatic diluent, mainly with feeds containing MSA or H_2SO_4. The number of data points clearly shows that the synergistic system is more popular in the literature, which is not surprising given its improved performance for the extraction step of a solvent extraction process. One of the downsides of this synergistic system is its reduced stripping efficiency, which tends to decrease as extraction efficiency increases.

The interaction parameters already included in the model did not yield an accurate prediction of acid extraction by the synergistic system (Fig. 13, top). The absence of direct binary interactions between 1-octanol and TEHA causes an underestimation of % *E*, indicating that there is some favourable interaction between 1-octanol and TEHA, enhancing the acid extraction. This observation matches the explanation of synergy in the amine-alcohol systems as described in the solvent extraction mechanism section above (§4.2). Therefore, short- and mid-range binary interaction parameters were introduced between 1-octanol and TEHA/TEHAH$^+$ (Table 2).

The short-range interaction parameters are embedded in the UNIQUAC equation, which governs the local composition around a species.[36] This can be roughly correlated to their first coordination sphere. These parameters are non-symmetrical, meaning that the interaction energy a_{ij} is not equal to a_{ji}. Thus, the interaction of a central species i with surrounding species j is not equal to the interaction of central species j with surrounding species i. a_{ij} and a_{ji} often have the same sign, *i.e.*, they are both positive for non-miscible species and negative when both species mix well. Values with opposite signs are fitted for a_{ij} and a_{ji} between 1-octanol and TEHA/TEHAH$^+$ (Table 2), underpinning the complex underlying chemical interactions. The negative a_{ij} values suggest that 1-octanol likes to be surrounded by TEHA and TEHAH$^+$, while TEHAH$^+$ and certainly TEHA do not want much 1-octanol in their direct vicinity. Overall, a net negative short-range interaction between 1-octanol and TEHAH$^+$ improves the extraction of acid in synergistic systems. The mid-range parameters account for non-ideal chemical interactions between neutral molecules and ions, or between, within and beyond the first coordination sphere. These were required between 1-octanol and TEHAH$^+$ to achieve a good fit, suggesting that 1-octanol influences the stability of (TEHAH$^+$)(X$^-$) in the outer spheres of the complex or the reverse micelles.[58–60]

The QoF graph improves significantly when interactions between TEHA and 1-octanol are included in the thermodynamic model (Fig. 13, bottom). Now, there is only the slightest indication of a lack of fit at low and high % *E*, which

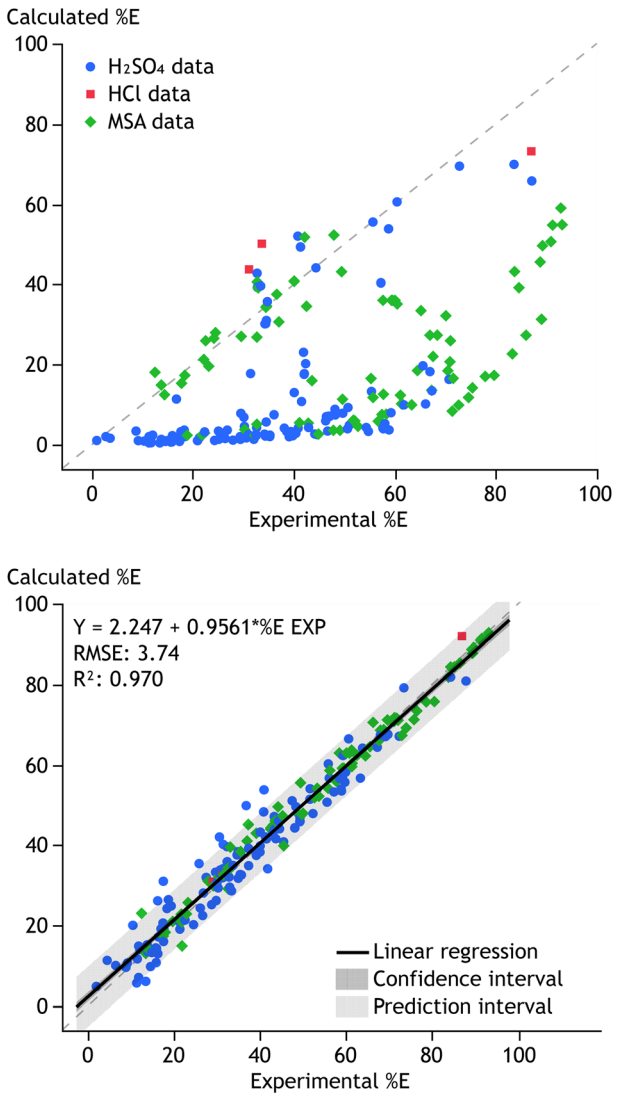

Fig. 13 Quality of fit graph for % *E* data of the synergistic system before (top) and after (bottom) optimisation. Statistical intervals are given with 95% confidence. The dashed grey line represents the ideal fit.

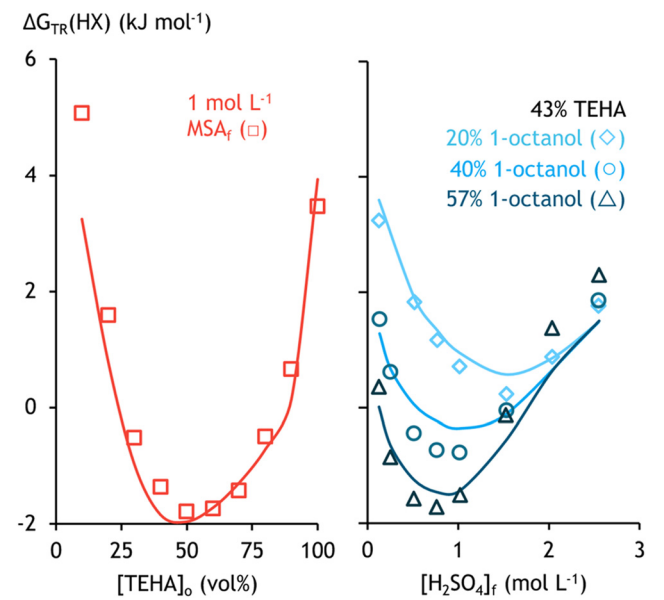

Fig. 14 Model fit (lines) of MSA and H_2SO_4 extraction mixtures of TEHA and 1-octanol (left) and 43 vol% TEHA in mixtures of 1-octanol and *n*-dodecane (right).[14,42]

originates rather from the very narrow confidence interval than from any problematic discrepancy between the model calculation and the data. A newly measured % E is expected to fall within an interval of ±7.5 with a 95% confidence (2 times RMSE).

The synergistic effect is clearly visible in the calculated extraction of 1 mol L^{-1} MSA by a mixture of TEHA and 1-octanol with varying concentrations measured by Kwok et al. (Fig. 14, left).[14] The distribution of MSA at 50 vol% TEHA is, with its −2 kJ mol^{-1}, more than 6 kJ mol^{-1} more efficient than that at 100 vol% 1-octanol or 100 vol% TEHA. Also for H_2SO_4 systems, the ΔG_{TR} is calculated significantly lower when n-dodecane is exchanged for 1-octanol at 43 vol% TEHA (Fig. 14, right).[42]

Fig. 15 gives an overview of the accuracy for the whole thermodynamic model and shows no evidence of a lack of fit for % E. The error on the mean % E is ±6.8 (95% confidence, two times RMSE), showing that the extraction of MSA, H_2SO_4, and HCl by single extractant and synergistic systems can be calculated with a confidence that falls in line with that of experimental data. The broadest distribution of residuals on % E is found for the TEHA-1-octanol (synergistic) system, likely due to its extensive coverage in the literature by multiple authors. This broad dataset increases the likelihood of systematic deviations within certain subsets of the data. For comparison, previously published thermodynamic models for acid extraction in solvent extraction systems have reported deviations between predicted and experimental values ranging from ±6% to ±21.3%.[80,81]

When all data is consolidated in one QoF graph, the thermodynamic model still slightly underestimates the highest values of $(O/A)_e$ and $(density)_o$ (Fig. 15). There are only a few data points available in this region, limited to systems with undiluted TEHA or undiluted 1-octanol at very high acid concentrations in the feed (>6.5 mol L^{-1}). Although this reduces the accuracy of the analysis in that region, it is of limited relevance for solvent extraction applications due to mutual solubility issues and higher viscosities. Below these

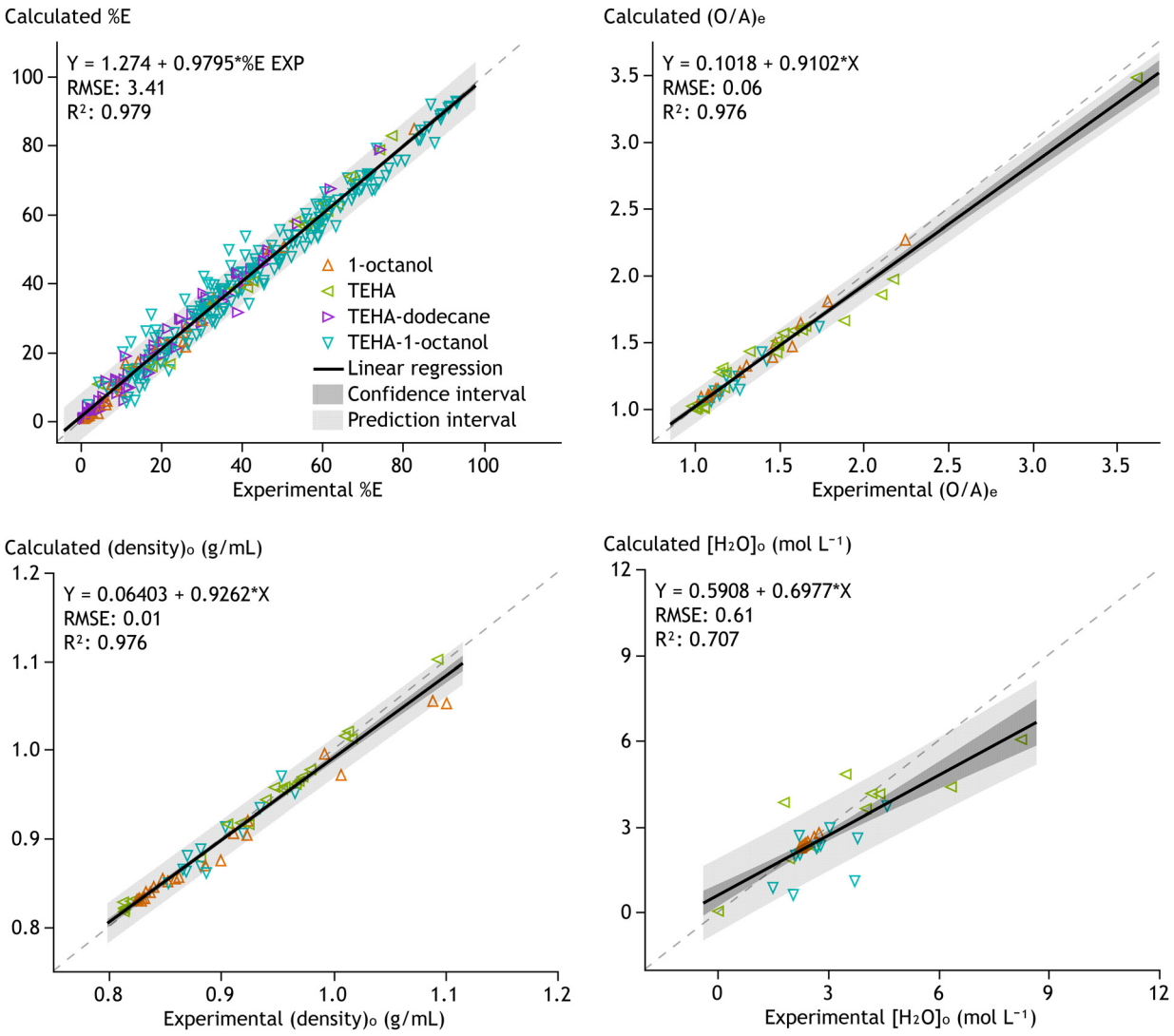

Fig. 15 Quality of fit graph for all data. Statistical intervals are given with 95% confidence. The dashed grey line represents the ideal fit.

extremities of high acid concentrations and undiluted TEHA or 1-octanol, no lack of fit is observed. Overall, the prediction interval is narrow with an error on the mean $(O/A)_o$ of ±0.12 and on $(density)_o$ of ±0.02 g mL^{-1}. Both are given with 95% confidence, calculated using RMSE.

The underestimation in the (O/A)e and (density)o QoF plots likely stems from the model undercalculating $[H_2O]_o$ in this region. The overall QoF graph for $[H_2O]_o$ shows significantly more deviation than the QoF graphs for the other aspects of the equilibrium (Fig. 15). Experimental measurement difficulties and limitations of the OLI-MSE framework contribute to these increased residuals and some lack of fit. Measuring $[H_2O]_o$ accurately is challenging due to the complexity of the organic phase, possible interference from co-extracted acid, and difficulties with avoiding environmental water during the whole measurement. Additionally, the framework is designed for homogeneous phases and cannot accurately capture the effect of reverse micelle formation in solvent extraction systems.[35] As a result, fitted interaction parameters may lack physical meaning. One example of this lack of physical meaning might be the use of mid-range interaction parameters between 1-octanol and $TEHAH^+$, on top of short-range interactions between these species (Table 2).

This study indicates that homogeneous-phase models can still accurately describe solvent extraction systems when the aggregation behaviour is relatively simple. Such aggregation behaviour could be the formation of spherical reverse micelles of constant size or cylindrical reverse micelles that vary only in length. In such scenarios, the interaction energies in the actual system and the corresponding interaction parameters in the thermodynamic model would be constant, even as the composition of the organic phases changes. Only the number of spherical reverse micelles or the length of cylindrical ones would vary, but that is captured by the mole fraction dependencies in the thermodynamic frameworks.[70] Consequently, incorporating aggregation behaviour in a semi-empirical MSE framework does not appear necessary to develop a predictive thermodynamic model for solvent extraction equilibria.

3.4. Thermodynamic model validation

The number of subsystems and variables in these subsystems complicates the division of the limited data available for the fitting procedure into training and validation datasets. Additionally, validating with data under the same conditions as the training set only tests the model's interpolation ability. Thermodynamic models that can extrapolate, or predictive models, are more useful for designing and optimising solvent extraction flowsheets. Hence, an experiment outside the training conditions was performed. This focuses on H_2SO_4 recovery from aqueous streams containing $NiSO_4$ by 40 vol% TEHA in 1-octanol, a system representative of industrial hydrometallurgical processes.[4]

Due to the absence of coordinating anions at the process conditions, no Ni(II) was extracted by TEHA and 1-octanol.

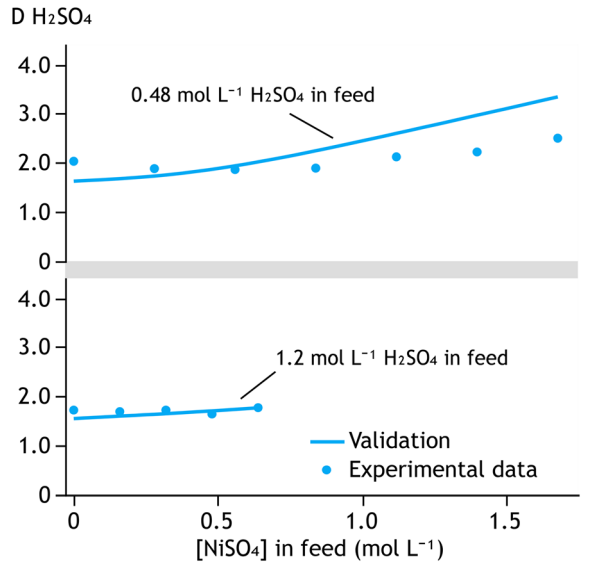

Fig. 16 Validation calculation (line) of experimental data (markers) on H_2SO_4 recovery from $NiSO_4$ solutions by 40 vol% TEHA in 1-octanol at 25 °C.

This was visually confirmed by the organic phase remaining completely colourless, while the aqueous phase was still dark green. Only a slight increase in experimental $D(H_2SO_4)$ was observed with increasing $NiSO_4$ concentration (Fig. 16 and SI Table S2). Although the salting-out effect would enhance extraction,[82] this is likely offset by a reduced $[H_3O^+]$ concentration due to SO_4^{2-} protonation from $NiSO_4$. The model predicts a slightly stronger increase in $D(H_2SO_4)$, but calculated and experimental values remain close.

Fig. 17 provides a more quantitative comparison, showing the 95% prediction interval and RMSE to evaluate the model's predictive accuracy. The ideal fit line falls within the prediction interval, showing no significant deviation between a new experiment and its prediction by the thermodynamic

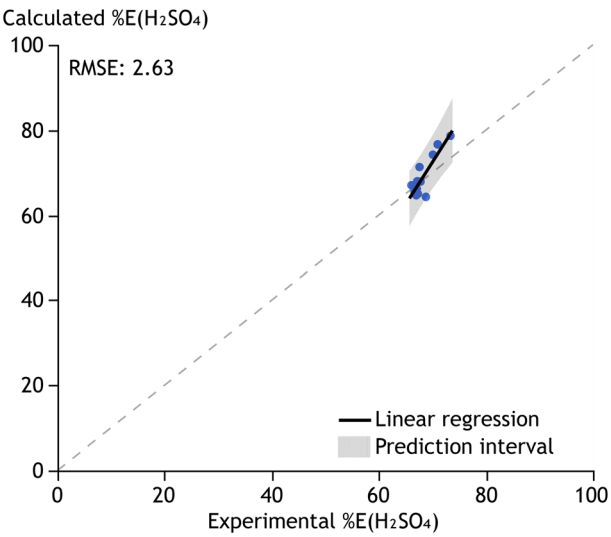

Fig. 17 Quality of fit graph for validation data. Statistical intervals are given with 95% confidence. The dashed grey line represents the ideal fit.

model, even when more representative hydrometallurgical streams with dissolved (leached) salts are used. The RMSE suggests a prediction error of ±5.3% *E* (95% confidence), well within the acceptable experimental error interval of ±10%.

4. Conclusions

This study demonstrates the development of a predictive thermodynamic model for the solvent extraction of H_2SO_4, HCl, and MSA using TEHA, 1-octanol, and their mixtures. The model, built within the OLI-MSE framework, integrates both literature and newly acquired experimental data to describe the complex equilibria and interactions in these systems. The extraction mechanism was investigated through FTIR spectroscopy and thermodynamic modelling. It involves reactive extraction by protonation of TEHA and non-reactive acid extraction above an equimolar ratio of HX : TEHA. The synergistic behaviour of TEHA and 1-octanol was investigated and mechanistically explained, with 1-octanol acting as both a phase modifier and a stabiliser of extractant–acid complexes. The model accurately reproduces acid distribution ratios, extraction efficiencies, liquid densities, and water uptake across a broad range of conditions. Furthermore, it reproduces synergistic effects by incorporating binary interaction energy parameters between TEHA and 1-octanol. Validation with recovery of H_2SO_4 from $NiSO_4$-containing feeds confirms its applicability to more realistic hydrometallurgical processes. The thermodynamic model retains its predictive accuracy despite not explicitly accounting for inverse micelle formation, which has been reported in the investigated solvent extraction systems. This outcome suggests that either such micelles are not significantly present under the studied conditions, or their effects are sufficiently captured through the existing semi-empirical framework without requiring an explicit description.

Author contributions

Rayco Lommelen: conceptualisation, data curation, formal analysis, investigation, methodology, validation, visualisation, writing – original draft. Koen Binnemans: conceptualisation, funding acquisition, resources, supervision, writing – review & editing.

Conflicts of interest

The authors declare that they have no known competing financial interests or personal relationships that could have appeared to influence the work reported in this paper.

Data availability

The data supporting this article have been included as part of the supplementary information (SI).

Supplementary information is available. See DOI: **https://doi.org/10.1039/d5re00386e**.

Acknowledgements

This work was funded by the European Union (ERC, CIRMET, project number 101093943). Views and opinions expressed are however those of the author(s) only and do not necessarily reflect those of the European Union or the European Research Council Executive Agency. Neither the European Union nor the granting authority can be held responsible for them. The authors acknowledge Dr Stijn Raiguel for the fruitful discussions on reverse micelles and his contributions to the analysis of the FT-IR spectra.

References

1 F. Crundwell, M. Moats, V. Ramachandran, T. Robinson and W. Davenport, *Extractive Metallurgy of Nickel, Cobalt and Platinum Group Metals*, Elsevier, Amsterdam, 2011.
2 A. Agrawal and K. K. Sahu, *J. Hazard. Mater.*, 2009, **171**, 61–75.
3 C. Agarwal and A. K. Pandey, *Environ. Sci.:Adv.*, 2023, **2**, 1306–1339.
4 M. L. Free, *Hydrometallurgy: Fundamentals and Applications*, John Wiley & Sons, Inc, Hoboken, New Jersey, 2016.
5 K. Binnemans and P. T. Jones, *J. Sustain. Metall.*, 2022, **9**, 26–45.
6 K. Binnemans and P. T. Jones, *J. Sustain. Metall.*, 2022, **9**, 1–25.
7 V. D. Talnikar and Y. S. Mahajan, *Korean J. Chem. Eng.*, 2014, **31**, 1720–1731.
8 J. Rydberg, M. Cox, C. Musikas and G. R. Choppin, *Solvent Extraction Principles and Practice, Revised and Expanded*, Marcel Dekker, New York, New York, 2nd edn, 2004.
9 U. Kesieme, A. Chrysanthou, M. Catulli and C. Y. Cheng, *J. Chem. Technol. Biotechnol.*, 2018, **93**, 3374–3385.
10 M. A. Muhsan and A. F. Zahoor, *Geosyst. Eng.*, 2023, **26**, 218–238.
11 A. M. Eyal and A. M. Baniel, *Solvent Extr. Ion Exch.*, 1991, **9**, 195–210.
12 J. Zhou, Y. Jia, C. Wei, H. Li and Y. Liu, *Sci. Rep.*, 2024, **14**, 30029.
13 M. Nango, A. Katayama and N. Kuroki, *Colloid Polym. Sci.*, 1974, **252**, 566–569.
14 W. C. Kwok, K. Binnemans and V. T. Nguyen, *MSc thesis*, KU Leuven, 2023.
15 A. Heidari, S. Shahryar, D. H. Fatmehsari and E. K. Alamdari, *Solvent Extr. Ion Exch.*, 2023, **41**, 810–825.
16 Z. Lu, S. Dourdain, B. Demé, J.-F. Dufrêche, T. Zemb and S. Pellet-Rostaing, *J. Mol. Liq.*, 2022, **349**, 118409.
17 J. Procházka, A. Heyberger and E. Volaufová, *Ind. Eng. Chem. Res.*, 2003, **42**, 5305–5311.
18 U. Kesieme, A. Chrysanthou, M. Catulli and C. Y. Cheng, *J. Environ. Chem. Eng.*, 2018, **6**, 3177–3184.
19 C. Bourget, M. Soderstrom, B. Jakovljevic and J. Morrison, *Solvent Extr. Ion Exch.*, 2011, **29**, 823–836.

20 BASF, Redbook Mining Solutions, **https://www.mining-solutions.basf.com/**, (accessed January 1, 2025).
21 L. Cohen, T. McCallum, O. Tinkler and W. Szolga, in *Extraction 2018*: The Minerals, Metals & Materials Series, 2018, pp. 2033–2045.
22 K. Wang, D. Peng, A. Alhadid and M. Minceva, *Ind. Eng. Chem. Res.*, 2024, **63**, 11110–11120.
23 M. Grabda, M. Panigrahi, S. Oleszek, D. Kozak, F. Eckert, E. Shibata and T. Nakamura, *Fluid Phase Equilib.*, 2014, **383**, 134–143.
24 M. Špadina, S. Dourdain, J. Rey, K. Bohinc, S. Pellet-Rostaing, J.-F. Dufrêche and T. Zemb, *Solvent Extr. Ion Exch.*, 2022, **40**, 106–139.
25 B. Zhuang, G. Ramanauskaite, Z. Y. Koa and Z.-G. Wang, *Sci. Adv.*, 2021, **7**, DOI: **10.1126/sciadv.abe7275**.
26 X. Lin, P. Ning, W. Xu, H. Cao and Y. Zhang, *Sci. China: Technol. Sci.*, 2015, **58**, 935–942.
27 S. Balasubramonian, N. K. Pandey and R. V. Subba Rao, *Prog. Nucl. Energy*, 2020, **128**, 103472.
28 H. Chen, A. J. Masters, R. Taylor, M. Jobson and D. Woodhead, *Ind. Eng. Chem. Res.*, 2019, **58**, 3822–3831.
29 C. O. Iloeje, C. F. J. Colón, J. Cresko and D. J. Graziano, *Environ. Sci. Technol.*, 2019, **53**, 7736–7745.
30 C. F. Baes, *Solvent Extr. Ion Exch.*, 2001, **19**, 193–213.
31 L. Miller and A. J. Gerbino, in *ALTA 2023 Uranium-Rare Earths Conference*, Perth, Australia, 2023.
32 L. Miller, M. Bagheri, P. Wang and S. Sequeira, in *ALTA 2024*, Perth, Australia, 2024.
33 R. Lommelen and K. Binnemans, *Sep. Purif. Technol.*, 2023, **313**, 123475.
34 R. Lommelen, B. Dewulf, J. Bussé and K. Binnemans, *Sep. Purif. Technol.*, 2024, **348**, 127708.
35 R. Lommelen and K. Binnemans, *ACS Omega*, 2021, **6**, 11355–11366.
36 P. Wang, A. Anderko and R. D. Young, *Fluid Phase Equilib.*, 2002, **203**, 141–176.
37 P. Wang, A. Anderko, R. D. Springer and R. D. Young, *J. Mol. Liq.*, 2006, **125**, 37–44.
38 N. Papaiconomou, J.-P. Simonin, O. Bernard and W. Kunz, *Phys. Chem. Chem. Phys.*, 2002, **4**, 4435–4443.
39 S. Ahmed, N. Ferrando, J.-C. de Hemptinne, J.-P. Simonin, O. Bernard and O. Baudouin, *Fluid Phase Equilib.*, 2018, **459**, 138–157.
40 N. Novak, G. M. Kontogeorgis, M. Castier and I. G. Economou, *Ind. Eng. Chem. Res.*, 2023, **62**, 13646–13665.
41 P. B. Gromov, A. G. Kasikov, E. A. Shchelokova and A. M. Petrova, *Hydrometallurgy*, 2018, **175**, 187–192.
42 D. F. Haghshenas, D. Darvishi, H. Rafieipour, E. K. Alamdari and A. A. Salardini, *Hydrometallurgy*, 2009, **97**, 173–179.
43 M. J. Ebrahimkhani, M. Azadian and H. Ghanadzadeh Gilani, *J. Chem. Eng. Data*, 2022, **67**, 404–415.
44 B. E. Lang, *J. Chem. Eng. Data*, 2012, **57**, 2221–2226.
45 K. Gottliebsen, B. Grinbaum, D. Chen and G. W. Stevens, *Hydrometallurgy*, 2000, **56**, 293–307.
46 A. M. Eyal, B. Hazan and R. Bloch, *Solvent Extr. Ion Exch.*, 1991, **9**, 211–222.
47 A. Eyal, B. Hazan and R. Bloch, *Solvent Extr. Ion Exch.*, 1991, **9**, 223–236.
48 U. K. Kesieme, H. Aral, M. Duke, N. Milne and C. Y. Cheng, *Hydrometallurgy*, 2013, **138**, 14–20.
49 M. Regadío, N. K. Batchu and K. Binnemans, *Chem. Eng. Res. Des.*, 2020, **161**, 304–311.
50 SciFinder, Tris(2-ethylhexyl)amine (CAS RN: 1860-26-0), **https://scifinder-n.cas.org**, (accessed July 17, 2025).
51 L. Zhong and S. F. Parker, *R. Soc. Open Sci.*, 2018, **5**, 181363.
52 B. Smith, *Spectroscopy*, 2019, **34**, 22–26.
53 U. K. Kesieme, H. Aral, M. Duke, N. Milne and C. Y. Cheng, *Hydrometallurgy*, 2013, **138**, 14–20.
54 E. Guerinoni, F. Giusti, S. Dourdain, J.-F. Dufrêche, R. Motokawa, Y. Ueda, N. Aoyagi, T. Zemb and S. Pellet-Rostaing, *J. Mol. Liq.*, 2024, **403**, 124820.
55 Z. Lu, S. Dourdain, B. Demé, J.-F. Dufrêche, T. Zemb and S. Pellet-Rostaing, *J. Mol. Liq.*, 2022, **349**, 118409.
56 D. S. Mathew and R.-S. Juang, *Sep. Purif. Technol.*, 2007, **53**, 199–215.
57 Z. Lu, S. Dourdain, J.-F. Dufrêche, B. Demé, T. Zemb and S. Pellet-Rostaing, *J. Mol. Liq.*, 2022, **349**, 118487.
58 Z. Lu, S. Dourdain and S. Pellet-Rostaing, *Langmuir*, 2020, **36**, 12121–12129.
59 Y. Liu, M. Lee and G. Senanayake, *J. Mol. Liq.*, 2018, **268**, 667–676.
60 J. Rey, S. Dourdain, J.-F. Dufrêche, L. Berthon, J. M. Muller, S. Pellet-Rostaing and T. Zemb, *Langmuir*, 2016, **32**, 13095–13105.
61 R. Nagarajan, *Langmuir*, 2002, **18**, 31–38.
62 J. J. Kosinski, P. Wang, R. D. Springer and A. Anderko, *Fluid Phase Equilib.*, 2007, **256**, 34–41.
63 J. W. Kang, K.-P. Yoo, H. Y. Kim, H. Lee, D. R. Yang and C. S. Lee, *Int. J. Thermophys.*, 2001, **22**, 487–494.
64 C. Mosselman and H. Dekker, *J. Chem. Soc., Faraday Trans. 1*, 1975, **71**, 417–424.
65 H. A. Gundry, D. Harrop, A. J. Head and G. B. Lewis, *J. Chem. Thermodyn.*, 1969, **1**, 321–332.
66 J. Chao and F. D. Rossini, *J. Chem. Eng. Data*, 1965, **10**, 374–379.
67 J. H. S. Green, *Chem. Ind.*, 1960, 1215–1216.
68 F. Veselý, P. Barcal, M. Zábranský and V. Svoboda, *Collect. Czech. Chem. Commun.*, 1989, **54**, 602–607.
69 H. C. Zegers and G. Somsen, *J. Chem. Thermodyn.*, 1984, **16**, 225–235.
70 J. Prausnitz, R. Lichtenthaler and E. G. de Azevedo, *Molecular Thermodynamics of Fluid-Phase Equilibria*, Pearson, Upper Saddle River, N.J, 3rd edn, 1998.
71 H. K. Hansen, P. Rasmussen, A. Fredenslund, M. Schiller and J. Gmehling, *Ind. Eng. Chem. Res.*, 1991, **30**, 2352–2355.
72 M. J. Dávila, R. Alcalde, M. Atilhan and S. Aparicio, *J. Chem. Thermodyn.*, 2012, **47**, 241–259.
73 J. L. Holmes and C. Aubry, *J. Phys. Chem. A*, 2011, **115**, 10576–10586.
74 J. L. Holmes and C. Aubry, *J. Phys. Chem. A*, 2012, **116**, 7196–7209.

75 E. S. Domalski and E. D. Hearing, *J. Phys. Chem. Ref. Data*, 1993, **22**, 805–1159.
76 M. Špadina, J.-F. Dufrêche, S. Pellet-Rostaing, S. Marčelja and T. Zemb, *Langmuir*, 2021, **37**, 10637–10656.
77 J. Xu, R. Paimin, W. Shen and X. Wang, *Fibers Polym.*, 2003, **4**, 27–31.
78 M. Góral, D. G. Shaw, A. Mączyński, B. Wiśniewska-Gocłowska and P. Oracz, *J. Phys. Chem. Ref. Data*, 2012, **41**, 043107.
79 P. G. T. Fogg and W. Gerrard, Solubility Data Series: Hydrogen Halides in Non-aqueous Solvent. IUPAC Analytical Chemistry Division, Oxford, UK, 1990, vol. 42.
80 K. Ziat, B. Mesnaoui, T. Bounahmidi, R. Boussen, M. de la Guardia and S. Garrigues, *Fluid Phase Equilib.*, 2002, **201**, 259–267.
81 B. Tan, C. Chang, D. Xu, Y. Wang and T. Qi, *ACS Omega*, 2020, **5**, 12174–12183.
82 R. Lommelen, B. Onghena and K. Binnemans, *Inorg. Chem.*, 2020, **59**, 13442–13452.